NASACR-177,348

A Reproduced Copy

OF

NASA CR-177,348

NASA CONTRACTOR REPORT 177348

(NASA-CR-177348) APPLICATION OF TWO-DIMENSIONAL UNSTEADY AERODYNAMIC TO A FREE-TIP ROTOR RESPONSE ANALYSIS (Kansas Univ. Center for Research, Inc.) 67 p
HC A04/MF A01 CSCL 01A G3/02

N85-29933

Unclas
29864

Application of Two Dimensional Unsteady Aerodynamics to a Free-Tip Rotor Response Analysis

Leslie Yates and Hiroyuki Kumagai

CONTRACT EE0193, NCC 2-175

May, 1985

NASA

NASA CONTRACTOR REPORT 177348

Application of Two Dimensional Unsteady Aerodynamics to a Free-Tip Rotor Response Analysis

Leslie Yates
Russmark Inc.
Cupertino, California

and

Hiroyuki Kumagai
The University of Kansas Center for Research Inc.
Lawrence, Kansas

CONTRACT EE0193, NCC 2-175

May, 1985

National Aeronautics and
Space Administration

Ames Research Center
Moffett Field, California 94035

TABLE OF CONTENTS

Application of Two Dimensional Unsteady Aerodynamics to a Free-Tip Rotor Response Analysis

Leslie Yates

Russmark Inc.
602 Stendhal Ln.
Cupertino, CA 95014

Hiroyuki Kumagai

The University of Kansas Center of Research Inc.
2291 Irving Hill Dr., Campus West
Lawrence, KS 66045-2969

Summary

The free-tip rotor utilizes a rotor blade tip which is structurally decoupuled from the blade inboard section. The tip is free to pitch about its own pitch axis to respond to the local flow angularity changes. The tip also experiences the heaving motion due to the flapping of the rotor blade. For an airfoil in any pitching and heaving motion which can be expanded into a Fourier series, the lift and moment calculated by Theodorsen's theory is simply the linear combination of the lift and moment calculated for each harmonic. These lift and moment are then used to determine the response of the free-tip rotor. A parametric study is performed to determine the effect of mechanical damping, mechanical spring, sweep, friction, and a constant control moment on the free-tip rotor response characteristics and the resulting azimuthal lift distributions. The results showed that the free-tip has the capability to suppress the oscillatory lift distribution around the azimuth and to eliminate a significant negative lift peak on the advancing tip. This result agrees with the result of the previous analysis based on the steady aerodynamics.

1. Introduction

For a helicopter in forward flight, there is a significant negative lift on the tip of the advancing blade. This combined with a positive lift on the retreating side causes an oscillatory lift loading which acts as a source of vibration. It has been suggested that a free-tip configuration could suppress the oscillatory azimuthal lift distributions at the tip and minimize this source of the vibration.

A free-tip rotor consists of a conventional inboard section with the outer five to fifteen percent of the blade allowed to pitch independently of the inner section of the blade (Figure 1). A more detailed discussion can be found in Reference 1 and 2. In programs FTR2 and HOVER, which compute the tip response in forward flight and the tip response to an air jet in hover respectively, Kumagai used a steady calculation for the lift coefficient, a constant moment coefficient at the 25% chord, and an aerodynamic damping factor calculated from the Quasi Vortex Lattice Method to study the behavior of the free-tip (Reference 1 and 2). His study indicated that the free-tip does indeed make the azimuthal lift distributions less oscillatory.

Boeing Vertol also developed a program to determine the behavior of the free-tip. In their program, B-65, the lift and moment are calculated from Theodorsen's theory for wings in pitching and heaving motion (Reference 3). The aerodynamic damping is automatically included in these calculations. In B-65 it is assumed that the local angle of attack, the inflow angle, the flapping angle, and the downwash velocity can all be approximated by a constant term and a sinusoidal term with the angular velocity of the rotor.

The purpose of the present study is to include Theodorsen's theory in the existing two dimensional numerical models, FTR2 and HOVER, and investigate its effects on the free-tip response characteristics. Although no modifications were made to the lift and moment derived from Theodorsen's theory, the local angle of attack, the inflow angle, the flapping angle, and the downwash velocity are all expanded into Fourier series, and the lift and moment are then uniquely determined for each harmonic. The computer programs developed to determine the response of the free-tip were UNSTEADY and UNSTHOVR.

For a small scale model in forward flight, the local angle of attack was calculated using three methods, FTR2, B-65, and UNSTEADY. The differences in the solutions are discussed in reference to the formulation of the three methods. For the same model in hover, the response to an air jet was examined using HOVER and UNSTHOVR.

For the small scale model and a full scale model, the effect of changing a number of parameters on the azimuthal lift distribution was studied. The parameters varied were the constant moment coefficient at the 25% chord, the constant control moment, the sweep in terms of the aerodynamic center offset of the free-tip from its pitch axis, the friction, the mechanical damping, and the mechanical spring constant.

2. List of Symbols

A_{0n}	Fourier coefficients of $\mathcal{L}(1)$
$A_{c_n m}$	Fourier coefficients of $\mathcal{L}(\cos n\omega t)$
$A_{s_n m}$	Fourier coefficients of $\mathcal{L}(\sin n\omega t)$
A_n, B_n	harmonic coefficients of α
b_α	aerodynamic damping coefficient $(lb\,ft\,sec/ft)$
b_θ	mechanical damping coefficient $(lb\,ft\,sec/ft)$
c_d	drag coefficient
c_l	lift coefficient
c_{l_α}	lift curve slope $(/rad)$
c_{l_0}	lift coefficient due to the steady part of the α, β, $\frac{dh}{dt}$, and ϕ
c_{l_n}	lift coefficient due to the n-th harmonic
c_m	moment coefficient
c_0	chord length (ft)
c_{pa}	location of the pitch axis measured from the leading edge in fraction of c_0
C_T/σ	rotor thrust coefficient
C_X/σ	rotor propulsive force coefficient
$\frac{dh}{dt}$	downwash velocity (ft/sec)
$\frac{dh_n}{dt}$	harmonic coefficients of the downwash velocity (ft/sec)
h	vertical location of the free-tip due to the heaving motion (ft)
i	pure imaginary number
J	moment of inertia for the free-tip per unit span $(slug\,ft^2/ft)$
k_α	aerodynamic spring coefficient $(lb\,ft/ft)$
k_θ	mechanical spring coefficient $(lb\,ft/ft)$

$\mathcal{L}$	operator acting upon a, defined by eq. (27)
ℓ_a, ℓ_f	reference lengths used in calculating the feathering moment (ft)
L_{tip}	span of the free-tip (ft)
m	mass of the free-tip $(slug/ft)$
M	Mach number
$\mathcal{M}$	operator acting upon ϕ, $\frac{dh}{dt}$ and β, defined by eq. (27)
$\mathcal{M}_m$, $\mathcal{M}_{cm}$, $\mathcal{M}_{sm}$	Fourier coefficients of $\mathcal{M}$
M_{ft}	moment measured at the quarter chord $(lb\,ft/ft)$
m_a, m_f	forward and aft masses contributing to the feathering moment $(lb\,ft/ft)$
M_{dh}	moment due to drag and the dihedral $(lb\,ft/ft)$
M_f	moment caused by friction $(lb\,ft/ft)$
M_s	moment caused by the aerodynamic spring $(lb\,ft/ft)$
M_{f_s}	feathering moment $(lb\,ft/ft)$
p	total pressure (lb/ft^2)
p_∞	total pressure at infinity (lb/ft^2)
q	dynamic pressure (lb/ft^2)
q_0	constant control moment $(lb\,ft/ft)$
R	radius of the rotor (ft)
t	time (sec)
U	velocity of the rotor blade tip (ft/sec)
U_∞	free stream velocity (ft/sec)
u, v, w	perturbation velocity (ft/sec)
V	forward velocity of the helicopter (ft/sec)
x, y, z	Cartesian coordinates (ft)

x_{ℓ_i}	location of a shed vortex (ft)
x_θ	location of the pitch axis measured from mid-chord of the airfoil (ft)
α	local angle of attack (rad)
α_0	constant term in the Fourier expansion of the local angle of attack (rad)
β	flapping angle (rad)
Δc	effective pitch axis offset, distance between pitch axis and effective aerodynamic center in fraction of the chord
$\Delta\Gamma$	strength of shed vortex
$\Delta\Gamma_0, \Delta\Gamma_n$	harmonic coefficients of $\Delta\Gamma$
Γ_{tip}	free-tip dihedral, positive down (rad)
θ	pitch angle of the free-tip measured from disk plane (rad)
μ	rotor advance ratio
μ_f	friction coefficient
ρ_∞	free stream air density ($slug/ft^3$)
σ	rotor solidity
Φ	velocity potential
Φ'	perturbation velocity potential
ϕ	inflow angle (rad)
ϕ_n	harmonic coefficients of the inflow angle (rad)
ψ	azimuthal angle (rad)
Ω	angular velocity of the rotor (rad/sec)
ω	angular velocity of airfoil pitching motion (rad/sec)

3. Formulations

3.1. Theodorsen's Lift and Moment Coefficients

For an airfoil in potential flow, the velocity potential can be defined as (Figure 2)

$$\Phi = U_\infty x + \Phi' \tag{1}$$

where $U_\infty x$ is the free stream velocity potential and Φ' is the perturbation velocity potential.

The pressure distribution on the surface of the airfoil is given by the unsteady, incompressible Bernoulli's equation,

$$\frac{p - p_\infty}{\rho_\infty} = -\frac{\partial \Phi'}{\partial t} - \frac{1}{2}\left((U_\infty + u)^2 + v^2 + w^2\right) + \frac{1}{2}U_\infty^2 \tag{2}$$

The vector (u, v, w) is the perturbation velocity vector. If the perturbation velocities are small with respect to the free stream velocity, this equation can be linearized to give

$$\frac{p - p_\infty}{\rho_\infty} = -\frac{\partial \Phi'}{\partial t} - U_\infty u \tag{3}$$

The lifting pressure is the difference in the pressure on the upper and lower surfaces of the wing,

$$\Delta p = -2\rho_\infty \left(\frac{\partial \Phi'_u}{\partial t} + U_\infty \frac{\partial \Phi'_u}{\partial x}\right) \tag{4}$$

where

$$\begin{aligned} \Phi'_u &= \Phi' \big|_{\text{upper surface}} \\ &= -\Phi' \big|_{\text{lower surface}} \end{aligned} \tag{5}$$

The perturbation velocity potential for an airfoil in pitching and heaving motion consists of three parts, the velocity potential due to the pitching motion, $\Phi(\theta)$, the velocity potential due to the heaving motion, $\Phi(h)$, and the velocity potential due to shed vortices, $\Phi(\Delta\Gamma)$. Following Theodorsen's derivation, these potentials evaluated on the surface of the airfoil are given by

$$\begin{aligned} \Phi(\theta) &= U_\infty \theta \sqrt{1 - x^2} + \frac{d\theta}{dt}\left(\frac{x}{2} - x_\theta\right)\sqrt{1 - x^2} \\ \Phi(h) &= \frac{dh}{dt}\sqrt{1 - x^2} \\ \Phi(\Delta\Gamma) &= \frac{\Delta\Gamma(x_0)}{2\pi} \tan^{-1}\left(\frac{\sqrt{1 - x^2}\sqrt{x_0^2 - 1}}{1 - x x_0}\right) \end{aligned} \tag{6}$$

where θ is pitch angle, x is the location on the airfoil, $\frac{dh}{dt}$ is the downwash velocity, and $\Phi(\Delta\Gamma)$ is the velocity potential for a vortex of strength $\Delta\Gamma$ at x_0 (Figure 2).

To meet the Kutta condition at the trailing edge, the perturbation potential must satisfy

$$\left.\frac{\partial\Phi'}{\partial x}\right|_{x=1} = \text{finite} \tag{7}$$

Letting $\Phi' = \Phi(\theta) + \Phi(h) + \Phi(\Delta\Gamma)$ and substituting into Equation (7) gives

$$\begin{aligned}\frac{-x}{\sqrt{1-x^2}}\left(U_\infty\theta + \frac{d\theta}{dt}\left(\frac{x}{2} - x_\theta\right) + \frac{dh}{dt}\right) \\ + \frac{1}{\sqrt{1-x^2}}\frac{1}{2\pi}\int_1^\infty \Delta\Gamma(x_0)\frac{\sqrt{x_0^2-1}}{x_0-x}\,dx_0 \\ + \frac{1}{2}\frac{d\theta}{dt}\sqrt{1-x^2}\Big|_{x=1} = \text{finite}\end{aligned} \tag{8}$$

For the above expression to be finite, the coefficient of $\frac{1}{\sqrt{1-x^2}}$ must be zero at $x = 1$. This defines an integral equation for the vortex strength density $\Delta\Gamma(x_0)$.

$$\frac{1}{2\pi}\int_1^\infty \Delta\Gamma(x_0)\sqrt{\frac{x_0+1}{x_0-1}}\,dx_0 = U_\infty\theta + \frac{d\theta}{dt}\left(\frac{1}{2} - x_\theta\right) + \frac{dh}{dt} \tag{9}$$

In the helicopter environment it is possible to expand θ and $\frac{dh}{dt}$ into the Fourier series

$$\begin{aligned}\theta &= \theta_0 + \sum_{n=1}^{\infty}\theta_n e^{in\Omega t} \\ \frac{dh}{dt} &= \frac{dh_0}{dt} + \sum_{n=1}^{\infty}\frac{dh_n}{dt}e^{in\Omega t}\end{aligned} \tag{10}$$

where Ω is the angular velocity of the rotor and the coefficients θ_n and $\frac{dh_n}{dt}$ are complex to allow for the phase angles.

Assuming that the vortices are carried away with the free stream velocity, the vortex density can be written as

$$\Delta\Gamma(x_0, t) = \Delta\Gamma\left(t - \frac{x_0}{U}\right) \tag{11}$$

This also can be expanded into a Fourier series,

$$\Delta\Gamma(x_0, t) = \Delta\Gamma_0 + \sum_{n=1}^{\infty}\Delta\Gamma_n e^{in\Omega(t - x_0/U)} \tag{12}$$

It should be noted that the "free stream" velocity for the helicopter rotor tip is in fact time dependent. It takes the form $U = \Omega R + V \sin \Omega t$. This time dependence will be ignored in the derivation of Theodorsen's lift and moment coefficients.

Substitution of the Fourier expansions of θ, $\frac{dh}{dt}$, and $\Delta\Gamma$ into Equation (9) gives

$$\frac{1}{2\pi}\int_1^\infty \left(\Delta\Gamma_0 + \sum_{n=1}^{\infty}\Delta\Gamma_n e^{in\Omega(t-x_n/U)}\right)\sqrt{\frac{x_0+1}{x_0-1}}\,dx_0 = U\theta_0 + \frac{dh_0}{dt} + \sum_{n=1}^{\infty}\left(U\theta_n + in\Omega\theta_n\left(\frac{1}{2}-x_\theta\right) + \frac{dh_n}{dt}\right)e^{in\Omega t} \tag{13}$$

Equation (13) can be solved for $\Delta\Gamma_n$ to give

$$\Delta\Gamma_0 = \frac{2\pi U\left(\theta_0 + \frac{1}{U}\frac{dh_0}{dt}\right)}{\int_1^\infty \sqrt{\frac{x_0+1}{x_0-1}}\,dx_0}$$

$$\Delta\Gamma_n = \frac{2\pi U\left(\theta_n + \frac{in\Omega\theta_n}{U}\left(\frac{1}{2}-x_\theta\right) + \frac{1}{U}\frac{dh_n}{dt}\right)}{\int_1^\infty \sqrt{\frac{x_0+1}{x_0-1}}e^{-in\Omega x_0/U}\,dx_0} \tag{14}$$

Since $\Delta\Gamma_n$ depends only upon n-th harmonic of θ and $\frac{dh}{dt}$, it is possible to write the the perturbation velocity potential as the linear combination of the velocity potentials for each harmonic.

$$\Phi' = \Phi_0 + \sum_{n=1}^{\infty}\Phi_n \tag{15}$$

where

$$\Phi_0 = U\left(\theta_0 + \frac{1}{U}\frac{dh_0}{dt}\right)\sqrt{1-x^2} + 2\pi U\left(\theta_0 + \frac{1}{U}\frac{dh_0}{dt}\right)\frac{\int_1^\infty \tan^{-1}\frac{\sqrt{1-x^2}\sqrt{x_0^2-1}}{1-xx_0}\,dx_0}{\int_0^\infty \sqrt{\frac{x_0+1}{x_0-1}}\,dx_0}$$

$$\Phi_n = U\left[\theta_n + \frac{in\Omega}{U}\left(\frac{x}{2} - x_\theta\right)\theta_n + \frac{1}{U}\frac{dh_n}{dt}\right]\sqrt{1-x^2} + 2\pi U\left[\theta_n + \frac{in\Omega}{U}\left(\frac{x}{2} - x_\theta\right)\theta_n + \frac{1}{U}\frac{dh_n}{dt}\right]\times \left[\frac{\int_1^\infty \tan^{-1}\frac{\sqrt{1-x^2}\sqrt{x_0^2-1}}{1-xx_0}\,dx_0}{\int_1^\infty \sqrt{\frac{x_0+1}{x_0-1}}e^{-in\Omega x_0/U}\,dx_0}\right] \tag{16}$$

Since small perturbations were assumed, the lifting pressure distribution on the airfoil is linear in $\frac{\partial\Phi'}{\partial t}$ and in $\frac{\partial\Phi'}{\partial x}$. Therefore, the lifting pressure can be written as the linear combination of the lifting pressures calculated for each harmonic,

$$\Delta p = -2\rho_\infty \sum_{n=0}^{\infty}\left(\frac{\partial\Phi_n}{\partial t} + U\frac{\partial\Phi_n}{\partial x}\right) \tag{17}$$

and the lift and moment coefficient for an arbitrary heaving and pitching motion can be written as the linear combination of Theodorsen's lift and moment coefficients for each harmonic.

$$c_l = c_{l_0} + \sum_{n=1}^{\infty} c_{l_n}$$
$$c_m = c_{m_0} + \sum_{n=1}^{\infty} c_{m_n} \tag{18}$$

The lift and moment coefficients used in this study were obtained from Reference 3 and

are as follows.

$$
\begin{aligned}
c_{l_0} &= c_{l_\alpha}\left[\theta_0 + \frac{1}{U}\frac{dh_0}{dt} + c_0(1-c_{pa})\frac{\Omega\beta}{U}\right] \\
c_{l_n} &= c_{l_\alpha}\left[\left(F - c_0(3/4 - c_{pa})\frac{Gn\Omega}{U}\right)\theta_n + \frac{G}{n\Omega U}\frac{d^2h_n}{dt^2} + \frac{F}{U}\frac{dh_n}{dt}\right. \\
&\quad + \left(c_0(3/4 - c_{pa})\frac{F}{U} + \frac{G}{n\Omega}\right)\left(\frac{d\theta_n}{dt} + \Omega\beta_n\right) \\
&\quad \left. + \frac{c_0}{4}\left(\left(\frac{d\theta_n}{dt} + \Omega\beta_n\right)\frac{1}{U} + \frac{1}{U^2}\frac{d^2h}{dt^2} - c_0(c_{pa} - 1/2)\frac{1}{U^2}\frac{d^2\theta_n}{dt^2}\right)\right]
\end{aligned}
\tag{19}
$$

and

$$
\begin{aligned}
c_{m_0} &= c_{l_\alpha}\left[(c_{pa} - 1/4)\left(\theta_0 + \frac{1}{U}\frac{dh_0}{dt} + c_0(3/4 - c_{pa})\frac{\Omega\beta_0}{U}\right)\right. \\
&\quad \left. + \frac{c_0}{4}(c_{pa} - 3/4)\frac{\Omega\beta_0}{U}\right]
\end{aligned}
$$

$$
\begin{aligned}
c_{m_n} &= c_{l_\alpha}\left[(c_{pa} - 1/4)\left(\left(F - c_0(3/4 - c_{pa})\frac{Gn\Omega}{U}\right)\theta_n + \frac{G}{n\Omega U}\frac{d^2h_n}{dt^2}\right.\right. \\
&\quad \left. + \frac{F}{U}\frac{dh_n}{dt} + \left(c_0(3/4 - c_{pa})\frac{F}{U} - \frac{G}{n\Omega}\right)\left(\frac{d\theta_n}{dt} + \Omega\beta_n\right)\right) \\
&\quad + \frac{c_0}{4}\left((c_{pa} - 3/4)\left(\frac{d\theta_n}{dt} + \Omega\beta_n\right)\frac{1}{U} + (c_{pa} - 1/2)\frac{d^2h_n}{dt^2}\frac{1}{U^2}\right. \\
&\quad \left.\left. - c_0\left(\frac{1}{32} + (c_{pa} - 1/2)^2\right)\left(\frac{d^2\theta_n}{dt^2} + \Omega\frac{d\beta_n}{dt}\right)\frac{1}{U^2}\right)\right]
\end{aligned}
\tag{20}
$$

F and G are functions of the reduced frequency k,

$$
k = \frac{c_0 n\Omega}{2U}
\tag{21}
$$

and are given by

$$
\begin{aligned}
F + iG &= \frac{\int_1^\infty \frac{x_0}{\sqrt{x_0^2-1}} e^{-ikx_0}\,dx_0}{\int_1^\infty \frac{x_0+1}{\sqrt{x_0^2-1}} e^{-ikx_0}\,dx_0} \\
&= \frac{J_1(k) - iY_1(k)}{J_1(k) + Y_0(k) - i(Y_1(k) - J_0(k))}
\end{aligned}
\tag{22}
$$

The J_i's and the Y_i's are i-th order Bessel functions of the first and second kind.

Plots of the lift and moment coefficients for sinusoidal pitching, sinusoidal heaving, and combined pitching and heaving motion are plotted in Figures 4 to 7. The experimental data was taken from Reference 4. These figures show that there is some discrepancy in the amplitude and phase of the lift and moment coefficients. This may be due to viscous effects which are ignored in Theodorsen's theory.

3.2. Equation of Motion for the Free-Tip

The pitch angle measured with respect to the disk plane is given by the differential equation

$$\frac{d^2\theta}{dt^2} + \frac{b_\theta}{J}\frac{d\theta}{dt} + \frac{k_\theta}{J}\theta = \frac{\sum \text{Moments}}{J} \tag{23}$$

where

b_θ =mechanical damping coefficient

k_θ =mechanical spring constant

The moment forces in the pitch angle equation include

q_0 =constant control moment

M_0 =aerodynamic moment at the quarter chord

$= c_{m_0} q c_0^2$

M_f =moment due to friction

$= \mu m \Omega^2 R \frac{\frac{d\theta}{dt}}{\left|\frac{d\theta}{dt}\right|}$

M_{fe} =feathering moment

$= -\Omega^2 \left(m_f l_f^2 + m_a l_a^2\right) \sin\theta$

M_s =aerodynamic spring

$= -\Delta c\, c_l\, q\, c_0^2$

M_{dh} =moment due to drag and dihedral

$= c_d\, q\, c_0 \left(\frac{L_{tip}}{2}\right) \sin\Gamma_{tip} \cos\theta$

The pitch angle measured with respect to the disk plane (Figure 3) is simply given in terms of the local angle of attack, α, and the inflow angle, ϕ, by

$$\theta = \alpha - \phi \tag{24}$$

The lift and moment coefficients given in Equations (19) and (20) indicate that they can each be broken into two terms, the first which is dependent only upon α, $\frac{d\alpha}{dt}$, and $\frac{d^2\alpha}{dt^2}$ and the second which is dependent only upon ϕ, $\frac{d\phi}{dt}$, $\frac{d^2\phi}{dt^2}$, $\frac{dh}{dt}$, $\frac{d^2h}{dt^2}$, β, and $\frac{d\beta}{dt}$. Letting

$$\begin{aligned} c_l &= c_l(\alpha) + c_l(\phi, \frac{dh}{dt}, \beta) \\ c_m &= c_m(\alpha) + c_m(\phi, \frac{dh}{dt}, \beta) \end{aligned} \tag{25}$$

and substituting into Equation (23) gives

$$\begin{aligned} &\frac{d^2\alpha}{dt^2} + \frac{b_\theta}{J}\frac{d\alpha}{dt} + \frac{k_\theta}{J}\alpha + \frac{c_l(\alpha)qc_0^2\Delta c}{J} - \frac{c_m(\alpha)qc_0^2}{J} \\ &\quad + \frac{\Omega^2(m_f l_f^2 + m_a l_a^2)}{J}\alpha = \frac{q_\alpha}{J} + \frac{d^2\phi}{dt^2} + \frac{b_\theta}{J}\frac{d\phi}{dt} + \frac{k_\theta}{J}\phi \\ &\quad - \frac{c_l(\phi, \frac{dh}{dt}, \beta)qc_0^2\Delta c}{J} + \frac{c_m(\phi, \frac{dh}{dt}, \beta)qc_0^2\Delta c}{J} \\ &\quad + \frac{\Omega^2(m_f l_f^2 + m_a l_a^2)}{J}\phi + \frac{M_f}{J} + \frac{M_{dh}}{J} \end{aligned} \tag{26}$$

or defining new operators, $\mathcal{L}$ and M,

$$\mathcal{L}(\alpha) = \frac{M(\phi, \frac{dh}{dt}, \beta)}{J} + \frac{\Delta M}{J} \tag{27}$$

where

$$\Delta M = M_{dh} + M_f \tag{28}$$

The function ΔM is not a linear function of α and its derivatives. It is, however, small with respect to the aerodynamic spring and can be ignored as a first approximation.

By expanding α into a Fourier series and noting that the operator $\mathcal{L}$ is of the form $A(t)\frac{d^2\alpha}{dt^2} + B(t)\frac{d\alpha}{dt} + C(t)\alpha$. Equation (27) can be written as

$$\begin{aligned} &\alpha_0\mathcal{L}(1) + \sum_{n=1}^{\infty} A_n\mathcal{L}(\cos n\Omega t) + \sum_{n=1}^{\infty} B_n\mathcal{L}(\sin n\Omega t) \\ &\qquad = \frac{M(\phi, \frac{dh}{dt}, \beta)}{J} \end{aligned} \tag{29}$$

Both $\mathcal{L}(f(t))$ and $M(f(t))$ can be expanded into Fourier series,

$$\begin{aligned}
\mathcal{L}(1) &= A_{00} + \sum_{m=1}^{\infty} A_{0m}\cos m\Omega t + \sum_{m=1}^{\infty} B_{0m}\sin m\Omega t \\
\mathcal{L}(\cos n\Omega t) &= A_{c_n 0} + \sum_{m=1}^{\infty} A_{c_n m}\cos m\Omega t + \sum_{m=1}^{\infty} B_{c_n m}\sin m\Omega t \\
\mathcal{L}(\sin n\Omega t) &= A_{s_n 0} + \sum_{m=1}^{\infty} A_{s_n m}\cos m\Omega t + \sum_{m=1}^{\infty} B_{s_n m}\sin m\Omega t \\
M &= M_0 + \sum_{m=1}^{\infty} M_{cm}\cos m\Omega t + \sum_{m=1}^{\infty} M_{sm}\sin m\Omega t
\end{aligned} \tag{30}$$

Substitution of these Fourier expansions into Equation (29) and solving for the Fourier coefficients of α gives an infinite system of linear equations.

$$\begin{aligned}
\alpha_0 A_{00} + \sum_{n=1}^{\infty} A_n A_{c_n 0} + \sum_{n=1}^{\infty} B_n A_{s_n 0} &= \frac{M_0}{J} \\
\alpha_0 A_{0m} + \sum_{n=1}^{\infty} A_n A_{c_n m} + \sum_{n=1}^{\infty} B_n A_{s_n m} &= \frac{M_{cm}}{J} \\
\alpha_0 B_{0m} + \sum_{n=1}^{\infty} A_n B_{c_n m} + \sum_{n=1}^{\infty} B_n B_{s_n m} &= \frac{M_{sm}}{J}
\end{aligned} \tag{31}$$

Two different computer programs were developed to solve for the Fourier coefficients of alpha. The first program, UNSTEADY was developed for a free-tip rotor in forward flight. The number of harmonic terms for α, β, ϕ, and $\frac{dh}{dt}$ was limited to ten. This reduces the infinite system of linear equations for the Fourier coefficients of α to twenty-one. The coefficients were then solved by using Gauss elimination. Once a solution was determined, the right hand side of the equation of motion was then corrected by ΔM, and the harmonic coefficients were redetermined. This procedure was iterated until the solution converged.

The second program was UNSTHOVR. This program determines the response of the free-tip to an air jet. The number of harmonics was limited to 30 which reduces the number of linear equations to sixty-one. The method of solution was identical to that of UNSTEADY.

4. Results

4.1. Small Scale Model

4.1.1. Rotor parameters and numerical model description

A small scale model with a rectangular free-tip was studied in both hover and forward flight. The rotor parameters selected for the analysis are

$$\text{Radius} = 8.40 \quad ft$$
$$\text{Chord length} = 0.56077 \quad ft$$
$$\text{Free-tip span} = 0.84 \quad ft$$
$$\text{Moment of inertia} = 0.388 \times 10^{-3} \quad slug\,ft^2/ft$$
$$\text{Average tip speed} = 700.0 \quad ft/sec$$
$$\text{Forward flight speed} = 0.0 \text{ and } 209.4 \quad ft/sec$$
$$q_0 = 5 \quad lb\,ft/ft$$
$$\mu = 0.0 \text{ and } 0.3$$
$$\text{Airfoil} : \text{V23010-1.58}$$

The parameters which contribute to the feathering moment are

$$m_f = 0.1133 \times 10^{-2} \quad slug/ft$$
$$m_a = 0.1012 \times 10^{-3} \quad slug/ft$$
$$l_f = 0.0075 \quad ft$$
$$l_a = 0.0840 \quad ft$$

Note that the parameters for the free-tip dimensions are two dimensional. The center of gravity of the free-tip is located at its pitch axis. For a forward flight velocity of $V = 209.4\ ft/sec$, the inflow and flapping angles were calculated by the Boeing Vertol B-65 program. Two sets of data for rotor blade flapping and inflow angle distribution at the tip were generated by B-65 with $C_T/\sigma \approx 0.08$ and $C_X/\sigma \approx 0.007$. Boeing Vertol B-65 is a three dimensional rotor performance prediction program for elastic blade rotors, employing the blade element theory (Reference 2). The first data set was computed with a conventional rectangular fixed tip rotor, and the second set with the free-tip, whose span length was 0.84 ft. When the inflow angle was computed with the B-65 for the free-tip rotor, it had an elastic inboard section, which is up to 90 % of the blade where the free-tip

starts. For fixed tip rotor. the entire blade was elastic. In both cases, the blade elasticity was prescribed in terms of the first elastic mode shape in flapwise bending and torsion. The free-tip and fixed tip have an identical planform. The inflow and flapping angles obtained from B-65 were then used in FTR2 and UNSTEADY. These two sets of data are referred as fixed tip inflow set and free-tip inflow set respectively from now on. The resulting local angles of attack from the prescribed inflow angle and the rigid blade flapping, calculated by FTR2, B-65, and UNSTEADY are shown in Figure 8 for the fixed tip inflow set and in Figure 9 for the free-tip inflow set.

It should be noted that the computer programs, FTR2 and UNSTEADY do not make iterations for the inflow angle. In other words, the resulting lift on the free-tip does not affect the inflow angle. This will limit the accuracy of the analysis. Even for the inflow angle generated for the free-tip, the inflow angle contains inherent inaccuracy because the data was generated by B-65, which ignored the higher harmonic lift oscillations.

For these two data sets. there is disagreement in the three solutions. This can be partially explained by the differences in the values used for the lift curve slope. This had its largest effect on the advancing side where the formula for the lift slope in FTR2 and UNSTEADY has a discontinuity in $\frac{\partial c_l}{\partial M}$. However, this can not account for all of the discrepancies since both FTR2 and UNSTEADY used the same lift curve slope.

The additional differences may be explained by the differences in the lift and moment coefficients used in each program. In B-65, Theodorsen's unsteady lift and moment coefficients were used. The assumption was made that the constant and first harmonic terms dominated the Fourier expansions of the angle of attack. the heaving motion, and the flapping motion. No attempt was made to treat the harmonics separately, instead, they were all treated as if they were the first harmonic.

In FTR2, the steady forms of the lift and moment coefficients were used. The damping coefficient was assumed to be the damping coefficient calculated for the first harmonic of UNSTEADY. Again. no attempt was made to treat the harmonic terms separately.

In UNSTEADY. Theodorsen's lift and moment are uniquely determined for each harmonic.

To determine what effect these differences in angle of attack distributions might have upon the solution, consider the case of hover with an air jet. Since U is constant and

$\frac{d^2\alpha}{dt^2} = -\sum_{n=1}^{\infty} n^2\Omega^2\alpha_n$, the lift and moment coefficients take the form

$$\begin{aligned} c_{l_0} &= C_0\,\alpha_0 \\ c_{l_n} &= C_n\,\alpha_n + D_n\,\frac{d\alpha_n}{dt} \end{aligned} \tag{32}$$

$$\begin{aligned} c_{m_0} &= H_0\,\alpha_0 \\ c_{m_n} &= H_n\,\alpha_n + K_n\,\frac{d\alpha_n}{dt} \end{aligned}$$

The operator $\mathcal{L}$ acting upon the n-th harmonic gives

$$\begin{aligned} \mathcal{L}(\alpha) = \frac{d^2\alpha}{dt^2} &+ \left(\frac{b_\theta}{J} + (\Delta c\,D_n - K_n)\,qc_0^2\right)\frac{d\alpha}{dt} \\ &+ \left(\frac{k_\theta}{J} + \frac{(\Delta c\,C_n - H_n)\,qc_0^2}{J}\right)\alpha \end{aligned} \tag{33}$$

or

$$\mathcal{L}(\alpha) = \frac{d^2\alpha}{dt^2} + \frac{b_\theta + b_\alpha}{J}\frac{d\alpha}{dt} + \frac{k_\theta + k_\alpha}{J}\alpha \tag{34}$$

where C_n, D_n, H_n, and K_n are constants determined from Theodorsen's lift and moment, and k_α and b_α are the aerodynamic spring constant and the aerodynamic damping. k_θ is a mechanical torsional spring and b_θ is a mechanical viscous damper.

For HOVER, C_n and H_n in the above equation are replaced by

$$\begin{aligned} C_n &= C_0 \\ H_n &= 0 \\ D_n &= D_1 \\ K_n &= K_1 \qquad \text{for } n = 1,\infty \end{aligned} \tag{35}$$

For B-65,

$$\begin{aligned} C_n &= C_1 \\ D_n &= D_1 \\ H_n &= H_1 \\ K_n &= K_1 \qquad \text{for } n = 2,\infty \end{aligned} \tag{36}$$

If the mechanical damping and mechanical spring are ignored, the equation for the n-th harmonic of α is

$$\frac{d^2\alpha_n}{dt^2} + \frac{b_\alpha}{J}\frac{d\alpha_n}{dt} + \frac{k_\alpha}{J}\alpha = |M_n|\sin(n\Omega t + \phi_n) \tag{37}$$

Since U is constant for hover, the terms $A_{s_n m}$, $A_{c_n m}$, $B_{s_n m}$, and $B_{c_n m}$ in Equation (31) are equal to zero unless $n = m$.

The amplitude of α_n is given by

$$|A_n| = \frac{|M|}{\sqrt{(k - n^2\Omega^2)^2 + (bn\Omega)^2}} \tag{38}$$

If the forcing terms for HOVER, B-65, and UNSTHOVR are equal, it is possible to determine the ratio of the A_n calculated by UNSTHOVR with respect to the A_n calculated by HOVER or B-65. In UNSTHOVR the flapping motion is identically set equal to zero. The results are shown in Table 1. Compared to the coefficients calculated by UNSTHOVR, HOVER overestimated A_n for the first four harmonics; B-65 overestimated the second through fourth terms. However, for the fifth through tenth harmonics, both FTR2 and B-65 badly underestimated A_n.

The forcing function M is also affected by the treatment of the higher harmonic terms. The function M includes lift and moment terms which are due to the inflow angle, the heaving motion, and the flapping angle. The lift and moment due the steady portion of the inflow angle cancel out the lift and moment due the steady portion of the heaving. However, this is not true of the higher harmonic terms.

In HOVER no correction was made to M to allow for these higher harmonic lift and moment terms. B-65 treated these corrections as if they were all first harmonic. For no mechanical damping and no mechanical spring, M becomes

$$\frac{d^2\phi}{dt^2} + \frac{b}{J}\frac{d\phi}{dt} + \frac{k}{J}\phi + \frac{\Omega^2(m_f l_f^2 - m_a l_a^2)}{J}\phi + \frac{q_a}{J} + \frac{\Delta M}{J} \tag{39}$$

where b and k are the damping and spring coefficients derived from the $c_l(\phi, \beta, \frac{dh}{dt})$ and $c_m(\phi, \beta, \frac{dh}{dt})$. Table 2 shows the ratios of the forcing function amplitudes and the harmonic coefficients for the angle of attack, α. Note that there is a sizable correction to the first harmonic term of M in UNSTHOVR.

4.1.2. Free-tip response to an air jet during hover

The free-tip response to a vertical air jet during hover is now investigated. The air jet is modeled as a change in inflow angle. For simplicity, inflow angle change across the air jet was assumed to be a half sine wave. Note that the frequency of the excitation due to the air jet can be changed by changing either the rotor angular velocity or the width of the air jet. In this study, the width of the air jet was selected to be a variable so that all rotor parameters can remain constant. Figure 10 shows the azimuthal lift distributions computed by HOVER, and Figure 11 by UNSTHOVR. The results from UNSTHOVR also

include the lift distributions when two different levels of damping were added. For these two cases, HOVER and UNSTHOVR, the inflow angle was prescribed as follows.

$$\begin{aligned} \phi &= 0^\circ && \text{for } 0^\circ \le \psi < 90^\circ \\ \phi &= 3^\circ \sin 6\Omega t && \text{for } 90^\circ \le \psi < 120^\circ \\ \phi &= 0^\circ && \text{for } 120^\circ \le \psi < 360^\circ \end{aligned}$$

There are significant differences in the solutions. The peak lift value for the HOVER calculation is much higher than UNSTHOVR. This occurs because the aerodynamic damping coefficient calculated for the first harmonic is less than one half of the aerodynamic damping coefficient calculated for the higher harmonics as shown in Table 1. Since the program HOVER ignores the higher harmonic terms, the lift distribution behaves as a simple underdamped oscillator. This is not the case with UNSTHOVR where each harmonic term has its own aerodynamic damping and spring coefficients. Note especially how the fifth or sixth harmonics are not damped out in Figure 11.

For Figures 12 and 13 the inflow angle was changed as follows.

$$\begin{aligned} \phi &= 0^\circ && \text{for } 0^\circ \le \psi < 90^\circ \\ \phi &= 3^\circ \sin 12\Omega t && \text{for } 90^\circ \le \psi < 105^\circ \\ \phi &= 0^\circ && \text{for } 105^\circ < \psi < 360^\circ \end{aligned}$$

Again, the result of UNSTHOVR includes the additional lift distributions with two levels of damping. In spite of the high excitation frequency, 12Ω, Figure 13 shows that the relatively low harmonic oscillation is not damped out, namely, the fifth harmonic. The lift distributions in Figures 11 and 13 suggest that the natural frequency of the system is between 5Ω and 6Ω. From Table 1, it is also possible to determine that the natural frequency for this system is somewhere between 5Ω and 6Ω. Figure 14 shows a difference between the square of the natural frequency of the system, $\frac{k_\beta}{I}$, and harmonics of the rotor angular velocity to the square, $(n\Omega)^2$. Interpolation of the data suggests that the natural frequency of the system, is approximately $5.2\Omega = 433.33\ rad/sec$. For both cases increasing the mechanical damping also decreases the amplitude of lift oscillations.

4.1.3. Free-tip response in forward flight

For forward flight, the effects of friction, mechanical damping and mechanical spring on the azimuthal lift distributions are investigated. The computations were carried out with two different inflow sets described previously. The fixed tip inflow set was used for Figures 15 to 17, and the free-tip inflow set for Figures 18 to 20. In all cases, there is a noticeable lift peak on the retreating side around $\psi = 300^\circ$ to 330°. This peak is caused by the dynamic pressure build-up. Since the dynamic pressure on the retreating side is small,

the aerodynamic spring on the free-tip, which determines the capability of the free-tip response, is also low. Therefore, the free-tip fails to respond to the fast dynamic pressure build-up beyond $\psi = 270°$, which results in the lift peak. This is the q-effect discussed in Reference 1 and 2. For both sets of inflow angle and flapping angle data there is a large amount of variation in the lift force on the advancing side. This variation can be smoothed out by decreasing the coefficient of friction (Figures 15 and 18) or by increasing the mechanical damping (Figures 16 and 19). Increasing the mechanical damping has the undesirable effect of making the free-tip slow to react and causes the peak to peak lift to increase.

Figures 17 and 20 indicate that increasing the mechanical spring constant helps to decrease the peak to peak lift with the fixed tip inflow set, since the q-effect is the dominant in the lift distribution and adding a mechanical spring increases the natural frequency and enables the tip to respond faster. With the inflow angle distributions generated by B-65 with the free-tip, the q-effect does not seem to be significant because of its inflow pattern, and adding mechanical spring causes larger oscillations on the advancing side due to underdamping, which was predicted by the unsteady lifting surface theory (Reference 1 and 2). There is no appreciable smoothing of the higher harmonic terms of the lift distribution by the inclusion of mechanical damping.

Although the rotor parameters were identical for the two small scale cases, the azimuthal lift distributions calculated for the two sets of inflow and flapping angles are dissimilar due to the difference in inflow pattern. The mean lift level calculated with the free-tip inflow set is higher than that calculated with the fixed tip data. The lift distribution with free-tip inflow set has more higher harmonic components than the lift distribution with the fixed tip inflow set, although its peak to peak lift is smaller than the peak to peak lift calculated for the fixed tip inflow set.

In Figures 21 and 22, the pitch angle of the free-tip computed with the fixed tip inflow set and free-tip inflow set are presented. The fixed tip inflow set produced a much larger peak value for the pitch angle. For the fixed tip inflow set, vortices shed from the tip of the inboard section do not exist. In the free-tip data, the effect of these vortices is included. The inclusion of these shed vortices causes an upwash component to be added into the inflow angle at the free-tip. For this model the upwash component was not large enough to make the inflow angle positive. It did, however, reduce the magnitude of the inflow angle on the retreating side. This caused the pitch angle to remain positive and to have a smaller peak value.

4.2. Full Scale Model

4.2.1. Rotor parameters

A parametric study was performed for a full scale model with a swept free-tip. The parameters of interest were the sweep, the constant control moment, a constant moment coefficient at 25% chord, the mechanical spring constant, mechanical damping, and friction. The criteria for success was a constant lift distribution.

The rotor parameters used in this study are

$$\begin{aligned}
\text{Radius} &= 28.0 \quad ft \\
\text{Chord length} &= 1.2657 \quad ft \\
\text{Free-tip span} &= 2.8 \quad ft/sec \\
\text{Moment of inertia} &= 0.02 \quad slug\,ft^2/ft \\
\text{Average tip speed} &= 650 \quad ft/sec \\
\text{Forward flight speed} &= 325 \text{ and } 95 \quad ft/sec \\
q_0 &= 40 \quad lb\,ft/ft \\
\mu &= 0.5 \text{ and } 0.15 \\
\text{Airfoil} &: \text{V23010-1.58}
\end{aligned}$$

The parameters for the feathering moment are

$$\begin{aligned}
m_f &= 0.1649 \times 10^{-1} \quad slug\,ft \\
m_a &= 0.4415 \times 10^{-2} \quad slug/ft \\
l_a &= 0.28 \quad ft \\
l_f &= 0.075 \quad ft
\end{aligned}$$

Note that the parameters for the free-tip dimensions are two dimensional. The center of gravity of the free-tip was again located at its own pitch axis. Two sets of data were used for the flapping and inflow angles. For the first set of data, the forward velocity was 325 ft/sec with the advance ratio of $\mu = 0.5$. The inflow angle was calculated by B-65 for a fixed tip with $C_T/\sigma \approx 0.08$ and $C_X/\sigma \approx 0.007$. No flapping angles were available.

For the second set of data, the forward flight velocity was 95 ft/sec with the advance ratio being $\mu = 0.15$. The flapping and pitching motions were obtained from flight test data for a Sicorsky S-58 helicopter with a fixed tip rotor (Reference 5). The thrust coefficient based on the weight of the helicopter, 11,500 lb was $C_T/\sigma \approx 0.08$. The inflow angle was calculated from the experimental lift and the pitch angle.

4.2.2. Free-tip response in high speed forward flight

The lift distributions calculated with the first set of data with $\mu = 0.5$ are presented in Figures 23 to 29. The lift distribution shows a large amount of oscillation on the advancing side. There is also a large peak in the lift distribution on the retreating side. This is the q-effect discussed previously. Increasing the friction coefficient to 0.2×10^{-2} reduces the amplitude of the lift distribution (Figure 23). This behavior is similar to what was observed in small scale model. Since the friction is dependent upon the sign of $\frac{d\alpha}{dt}$, it acts as a damping term. When the motion is underdamped, additional friction helps to smooth out the lift distribution. When the motion is overdamped, additional friction contributes to the oscillatory lift distribution by further suppressing the capability of the free-tip to respond to the perturbations.

The inclusion of mechanical damping smooths out some of the higher frequency oscillations (Figure 24). As was the case with the small scale model, large mechanical damping prevents the free-tip from reacting quickly and causes the peak to peak lift to increase.

Inclusion of a mechanical spring has little or no effect on smoothing the higher frequency oscillations on the advancing side (Figure 25). However, it did have a major effect on flattening the lift distribution on the retreating side, since the mechanical spring helps to minimize the q-effect where the aerodynamic spring term is low.

Decreasing the effective pitch axis offset from the aerodynamic center of the free-tip had a drastic effect upon the lift distribution. Decreasing the effective pitch axis decreases the aerodynamic spring and damping. This allows the free-tip to oscillate with a larger amplitude as indicated in Figure 26.

The major effect of lowering the constant control moment was to lower the average lift (Figure 27). There are some small changes in the shape of the lift distribution, but very little smoothing occurs.

The inclusion of a constant aerodynamic moment coefficient at the 25% chord predominantly changes the lift on the advancing side (Figure 28). The positive c_m raises the lift and the negative c_m lowers the lift. There is no smoothing effect.

It appears that to obtain a constant lift distribution, both mechanical damping and a mechanical spring must be added. The mechanical damping is used to smooth the lift distribution on the advancing side; the mechanical spring is used to smooth the lift distribution on the retreating side. Both the mechanical spring and damping must be added since the mechanical damping causes a larger q-effect on the retreating side and the mechanical spring causes more lift oscillation on the advancing side. The combination of mechanical damping and mechanical spring are shown in Figure 29. This combination does indeed smooth the entire lift distribution and decrease the peak to peak lift, since it increases the natural frequency of the tip, without changing the damping characteristics.

4.2.3. Free-tip response in low speed forward flight

The lift distributions calculated with the second set of data with $\mu = 0.15$ are plotted in Figure 30, with three different levels of mechanical damping. The experimental set of data produced a much flatter distribution than the previous set of data for the high speed flight for all three levels of damping. This occurred because the higher order harmonic terms in the inflow angle, the downwash velocity, and the forward velocity are smaller than those in high speed data set with $\mu = 0.5$.

5. Conclusions

Two computer programs, UNSTEADY and UNSTHOVR were developed for the investigation of the free-tip rotor response during forward flight and hover. They both incorporate Theodorsen's lift deficiency functions, uniquely defined for each harmonic component of the free-tip pitching and heaving motion.

A large pitch axis offset of the free-tip from its aerodynamic center increases the aerodynamic spring, which improves the free-tip response. The addition of the mechanical spring reduces the q-effect on the retreating side. Mechanical damping must be added to minimize the oscillation on the advancing side. Neither the mechanical spring nor the damping should be large since the mechanical spring increases the amplitude of the oscillation on the advancing side and mechanical damping increases the q-effect. This result agrees with those cited in Reference 1 and 2. The calculations indicate that to achieve a constant lift distribution, both mechanical damping and a mechanical spring must be added.

Even with the higher harmonic terms on the advancing side, the lift distribution for the free-tip is much more constant than the lift distribution for the conventional fixed tip. It does not have a large negative lift on the advancing side. This alone should reduce some of the oscillation associated with the fixed tip rotor.

The higher harmonic terms of the angle of attack, the heaving motion and the forcing function in Theodorsen's theory were ignored in FTR2 and B-65. These progarms treated the lift and moment as if there was only a first harmonic motion.

It should also be noted that the inflow and flapping angles played a major role in the azimuthal variation of the lift coefficient as indicated by the differences in the azimuthal lift distributions of the two small scale models. Both models shared the same physical dimensions and the same forward velocity, however, the inflow and flapping angles were different. The lift distribution calculated with the free-tip inflow set had a higher average lift, a smaller peak to peak lift, and larger higher harmonic terms than the lift distribution calculated with the fixed tip inflow set.

The free-tip calculation of the inflow and flapping angles by B-65 treated all harmonic terms as if they were a first harmonic. In UNSTEADY and UNSTHOVR, the computer program was not iterated for the resulting lift and inflow angle, therefore, it is impossible to predict how the correct treatment of each harmonic term would affect the inflow and flapping angles and, hence, the azimuthal lift distribution. This should be seriously considered when examining the full scale results. The full scale inflow and flapping angles are either taken from a program which had a fixed tip or they are taken from experimental data for a fixed tip rotor. The wake relaxation of the total rotor system with the correct treatment of higher harmonics should be performed to solve this problem.

6. References

1. Kumagai, H., *"A Feasibility Study of Free-Tip Rotor Application as a Passive Cyclic Control Device"*, D.E. Thesis, Department of Aerospace Engineering, The University of Kansas, 1984

2. Kumagai, H., *"Parametric Analysis of a Passive Cyclic Control Device for Helicopters"*, NASA CR 166608, October, 1984

3. Boeing Vertol Company, *"Aeroelastic Rotor Analysis Program, C-60"*, Boeing Vertol Document No. D201-10378-1, May, 1974

4. Halfman, R. L., *"Experimental Aerodynamic Derivatives of a Sinusoidally Oscillating Airfoil in Two-Dimensional Flow"*, NACA Report 1108, 1952

5. Scheiman, J., *"A Tabulation of Helicopter Rotor-Blade Differential Pressures, Stresses, and Motion as Measured in Flight"*, NASA TM X-952, 1964

Tables and Figures

List of Tables

List of Figures

Table 1. Ratios of the harmonic coefficients

COEFFICIENT RATIOS				
HARMONIC	$\frac{b_n}{J}$	$\frac{k_n}{J} - (n\Omega)^2$	$\frac{\lvert A^{(3)}\rvert}{\lvert A^{(1)}\rvert}$	$\frac{\lvert A^{(3)}\rvert}{\lvert A^{(2)}\rvert}$
1	54.07	226,947	0.940	1.000
2	135.58	192,852	0.880	0.941
3	180.87	146,599	0.823	0.892
4	210.18	87,830	0.812	0.905
5	230.58	16,128	1.248	1.514
6	245.58	-68,856	5.195	4.471
7	256.59	-167,395	2.310	2.024
8	265.20	-279,695	1.659	1.549
9	272.97	-405,915	1.434	1.372
10	277.39	-546,176	1.323	1.282

$A^{(1)}$ is the value calculated by HOVER
$A^{(2)}$ is the value calculated by B-65
$A^{(3)}$ is the value calculated by UNSTHOVR

Table 2. Corrections to the forcing function

COEFFICIENT RATIOS		
HARMONIC	$\frac{M(\text{UNSTHOVER})}{M(\text{HOVER})}$	$\frac{A(\text{UNSTHOVER})}{A(\text{HOVER})}$
1	1.100	1.034
2	1.064	0.936
3	1.040	0.856
4	1.023	0.831
5	1.011	1.262
6	1.002	5.205
7	0.995	2.298
8	0.989	1.641
9	0.985	1.412
10	0.981	1.298

Figure 1. Free-tip rotor schematics

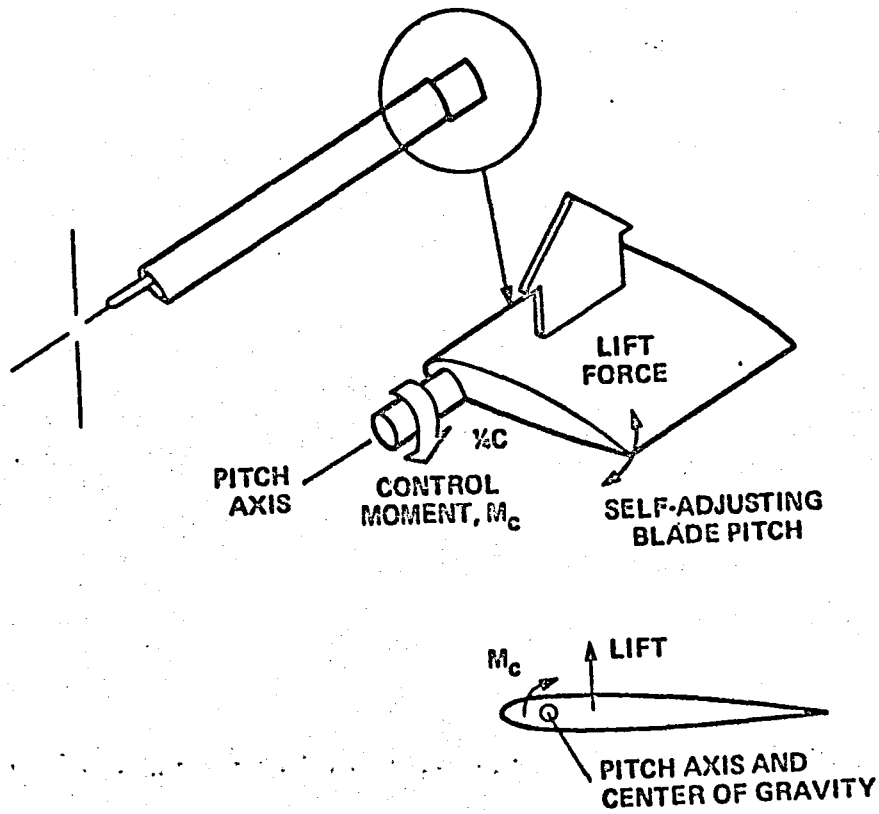

Figure 2. Geometry for Theodorsen's Theory

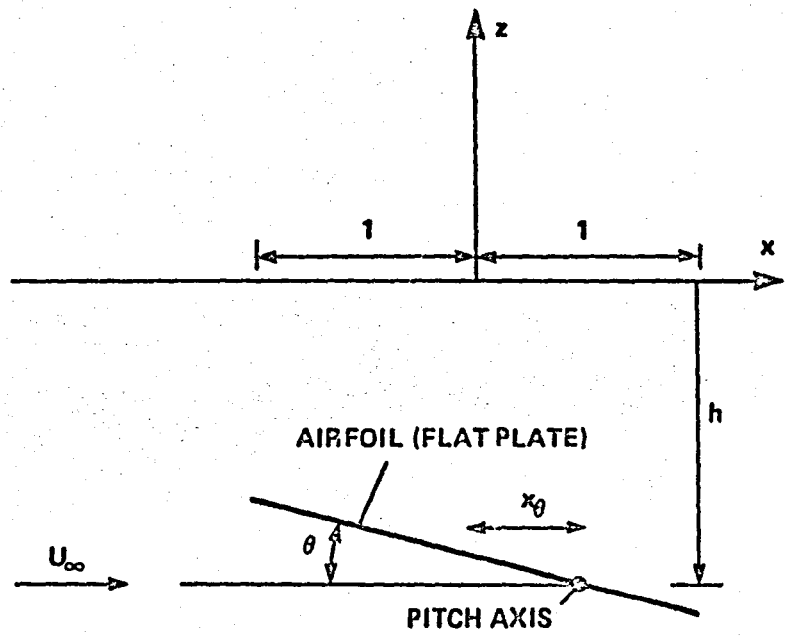

Figure 3. Definition of Angles

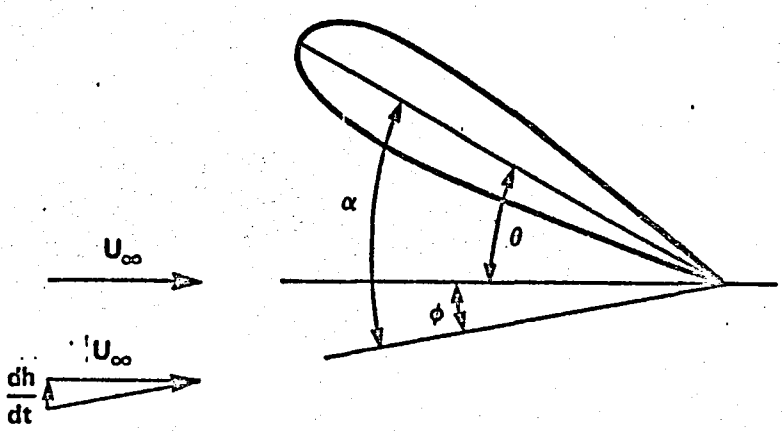

Figure 4. Lift coefficient for pitching, $\alpha = 0^\circ \pm 13.5^\circ$, $k = 0.2$

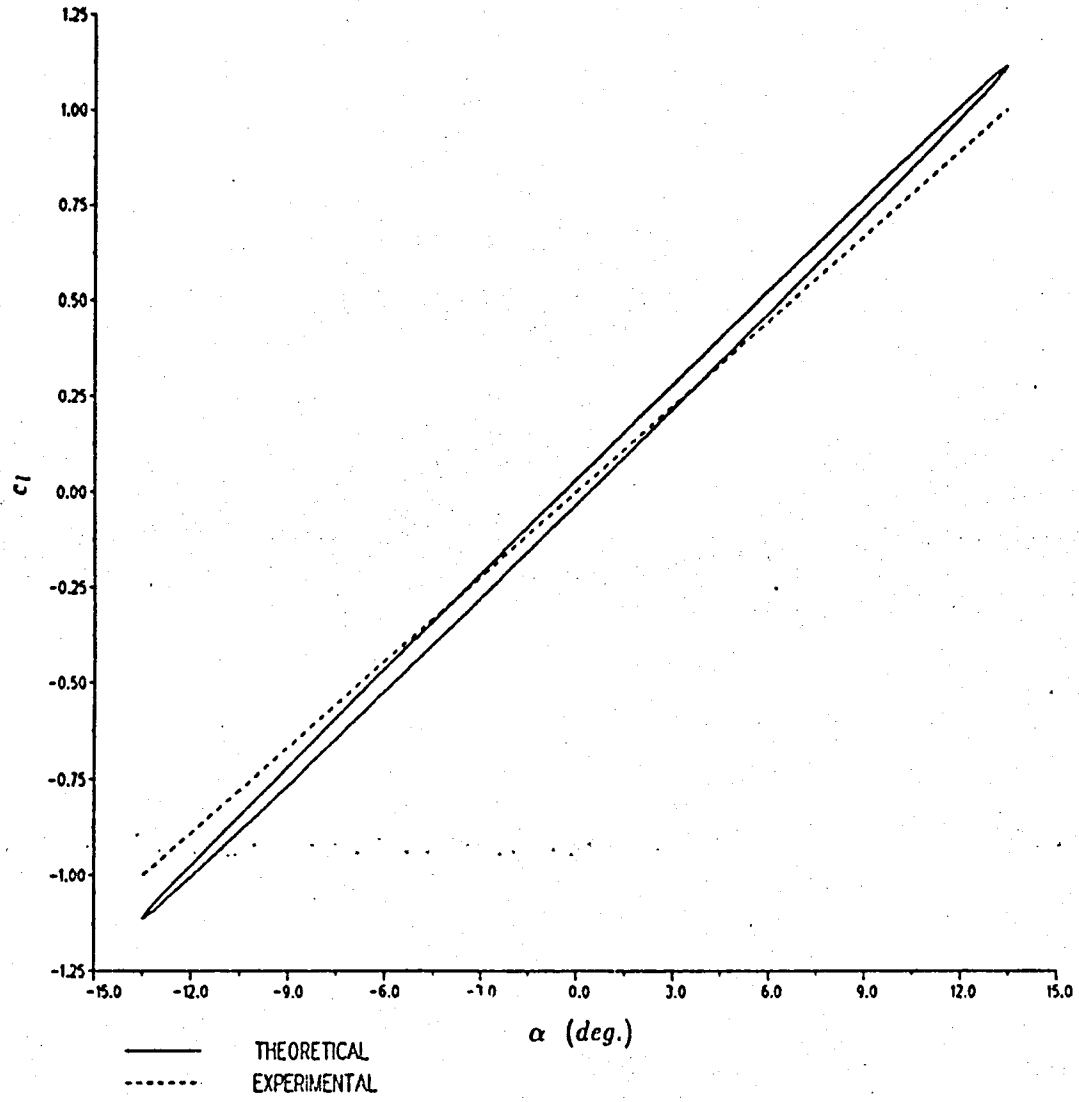

Figure 5. Lift coefficient for pitching and heaving, $\alpha = 0^\circ \pm 13.5^\circ$, $h/c = 0 \pm 0.1125$, $k = 0.2$

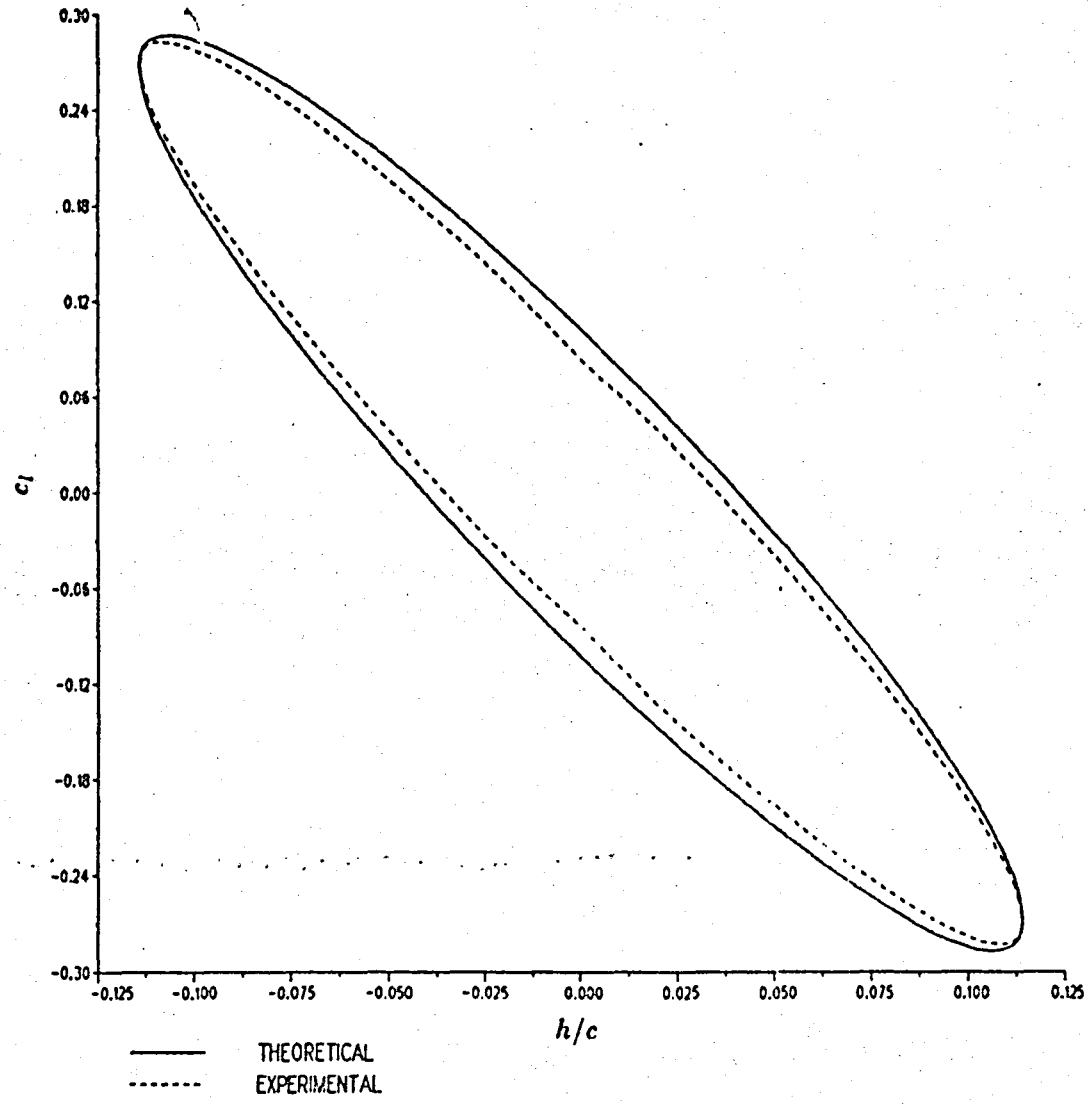

Figure 6. Moment coefficient for pitching, $\alpha = 0° \pm 13.5°$, $k = 0.2$

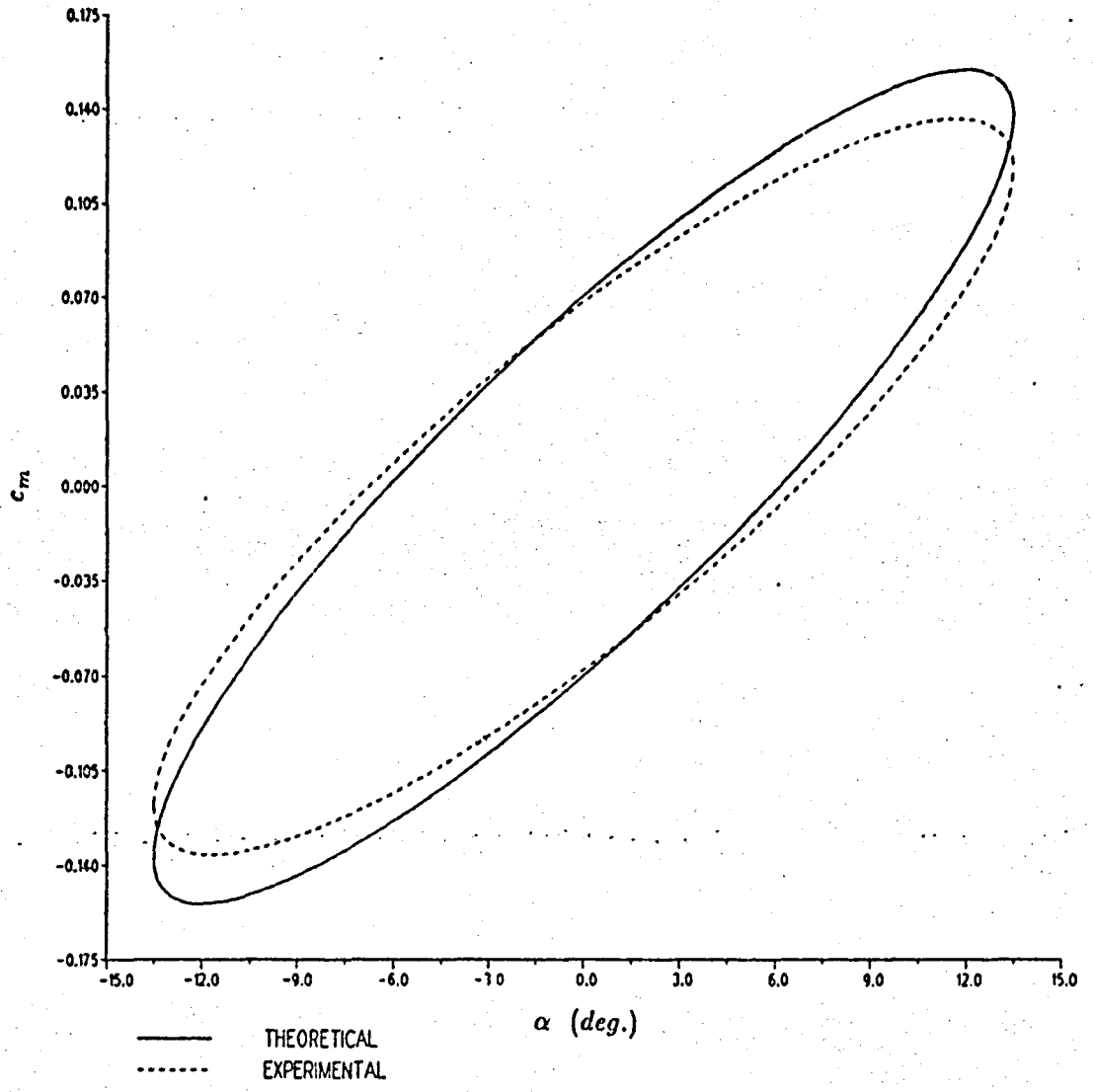

Figure 7. Moment coefficient for pitching and heaving, $\alpha = 0° \pm 13.5°$, $h/c = 0 \pm 0.1125$, $k = 0.2$

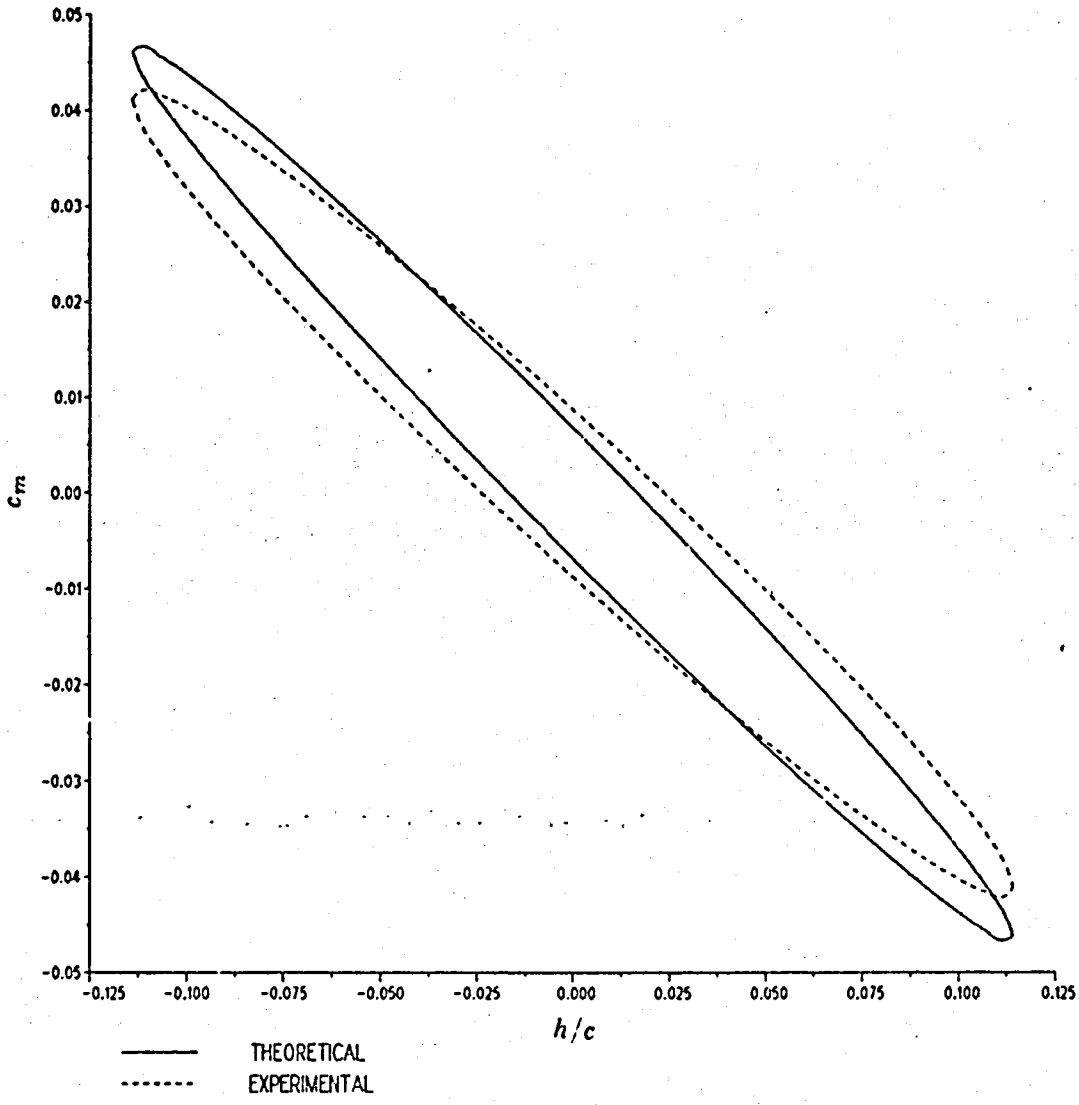

Figure 8. Angle of attack for fixed tip inflow set

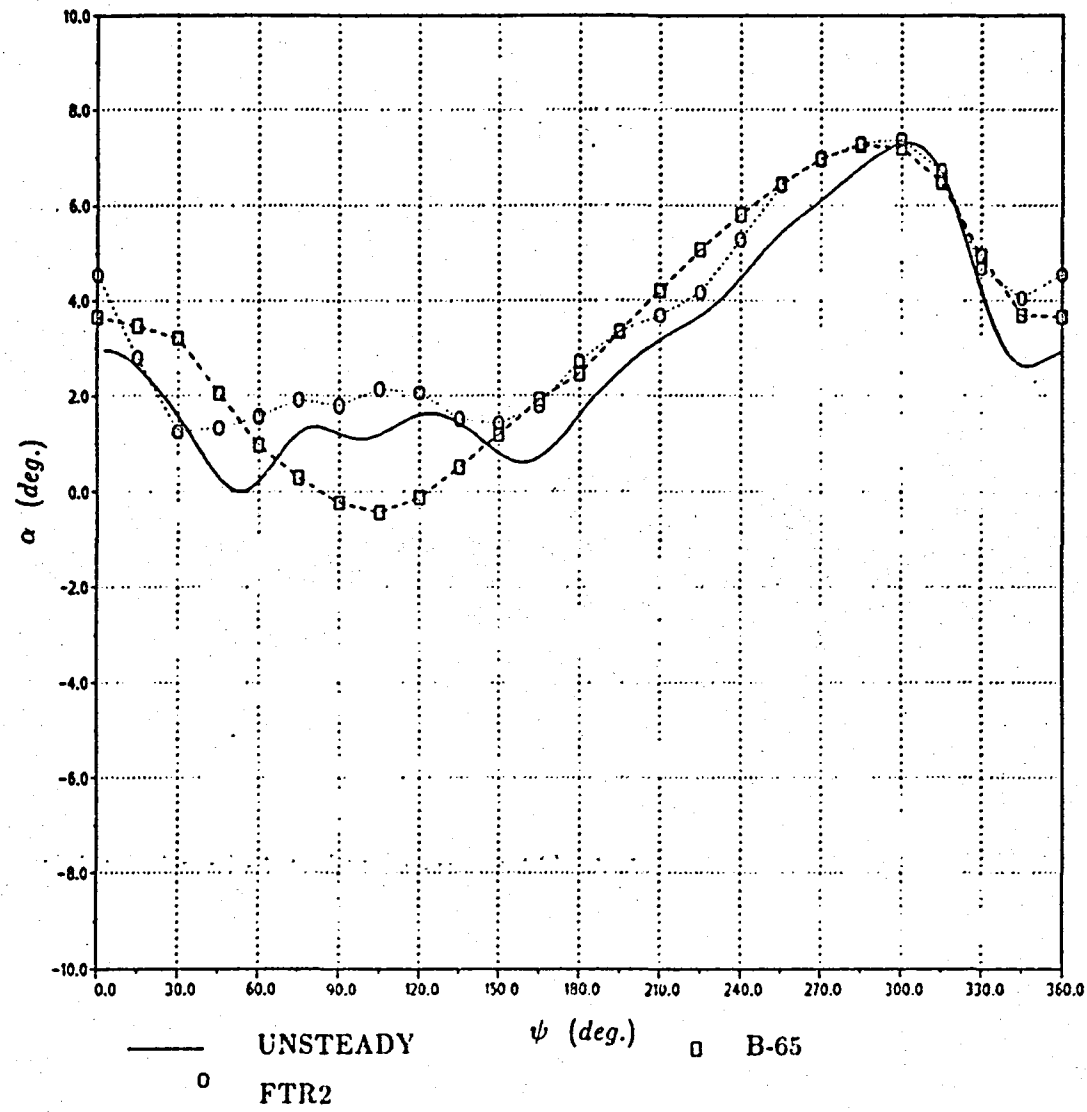

Figure 9. Angle of attack for free-tip inflow set

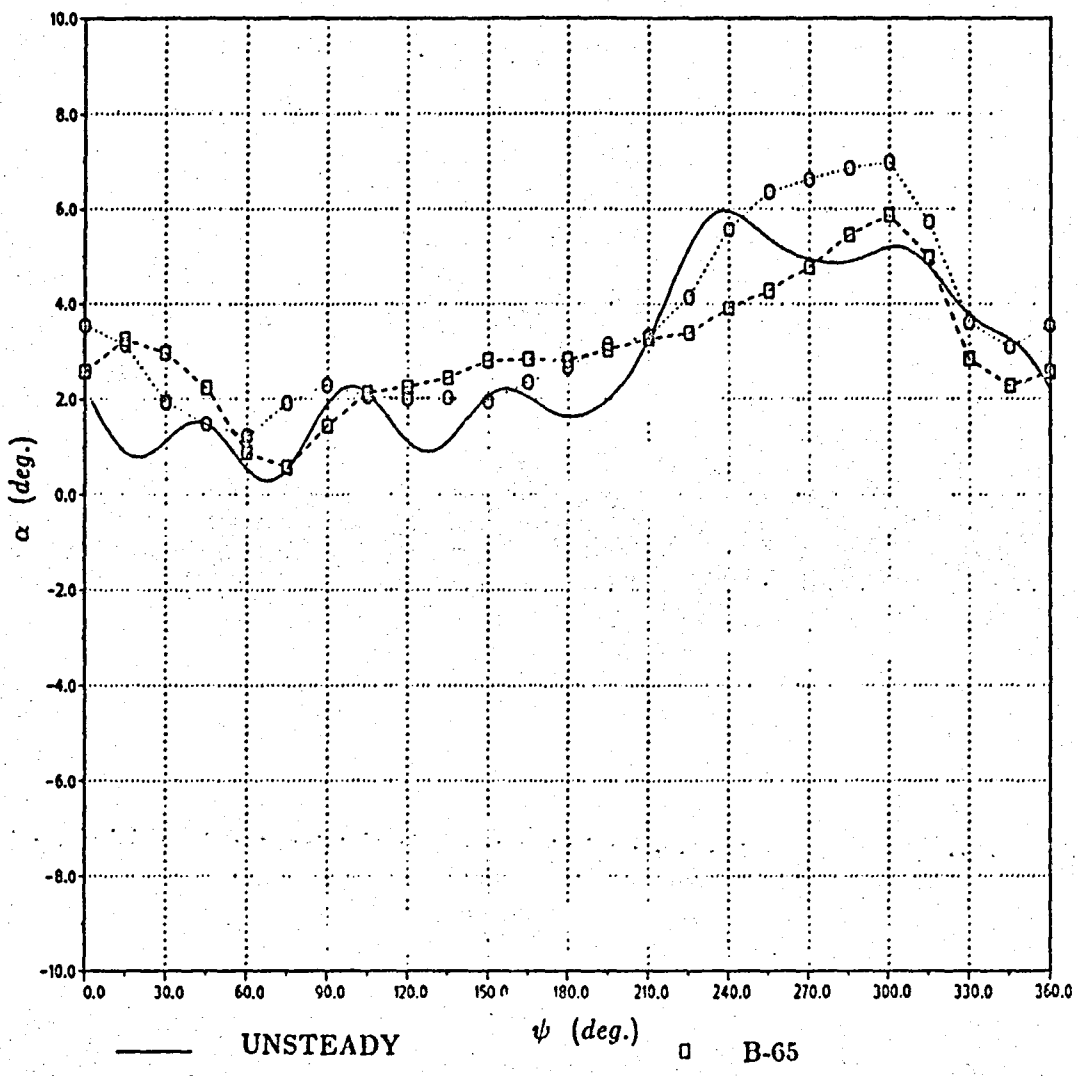

Figure 10. Response to an air jet, HOVER

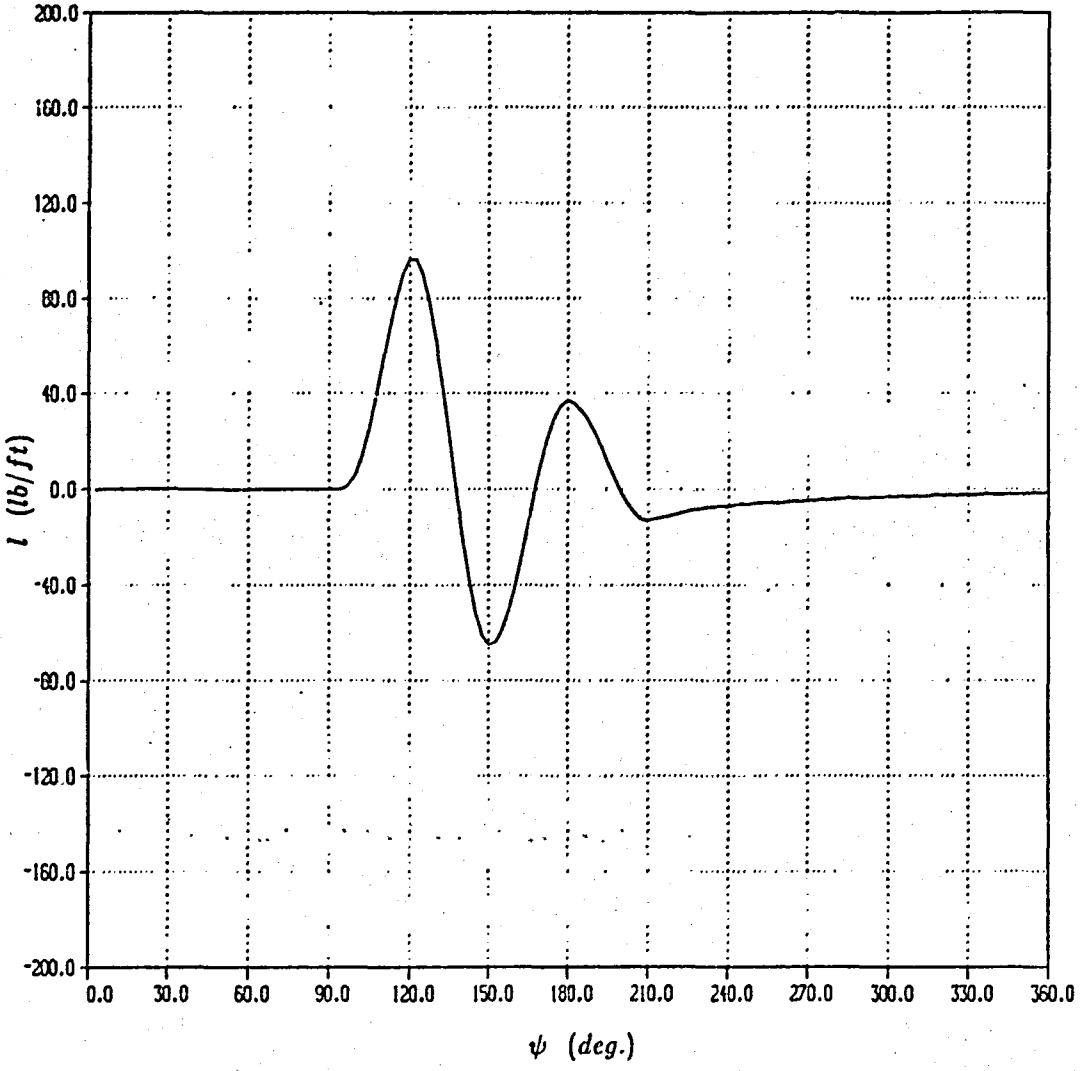

$b_\theta = 0.0$

Figure 11. Response to an air jet, UNSTHOVR

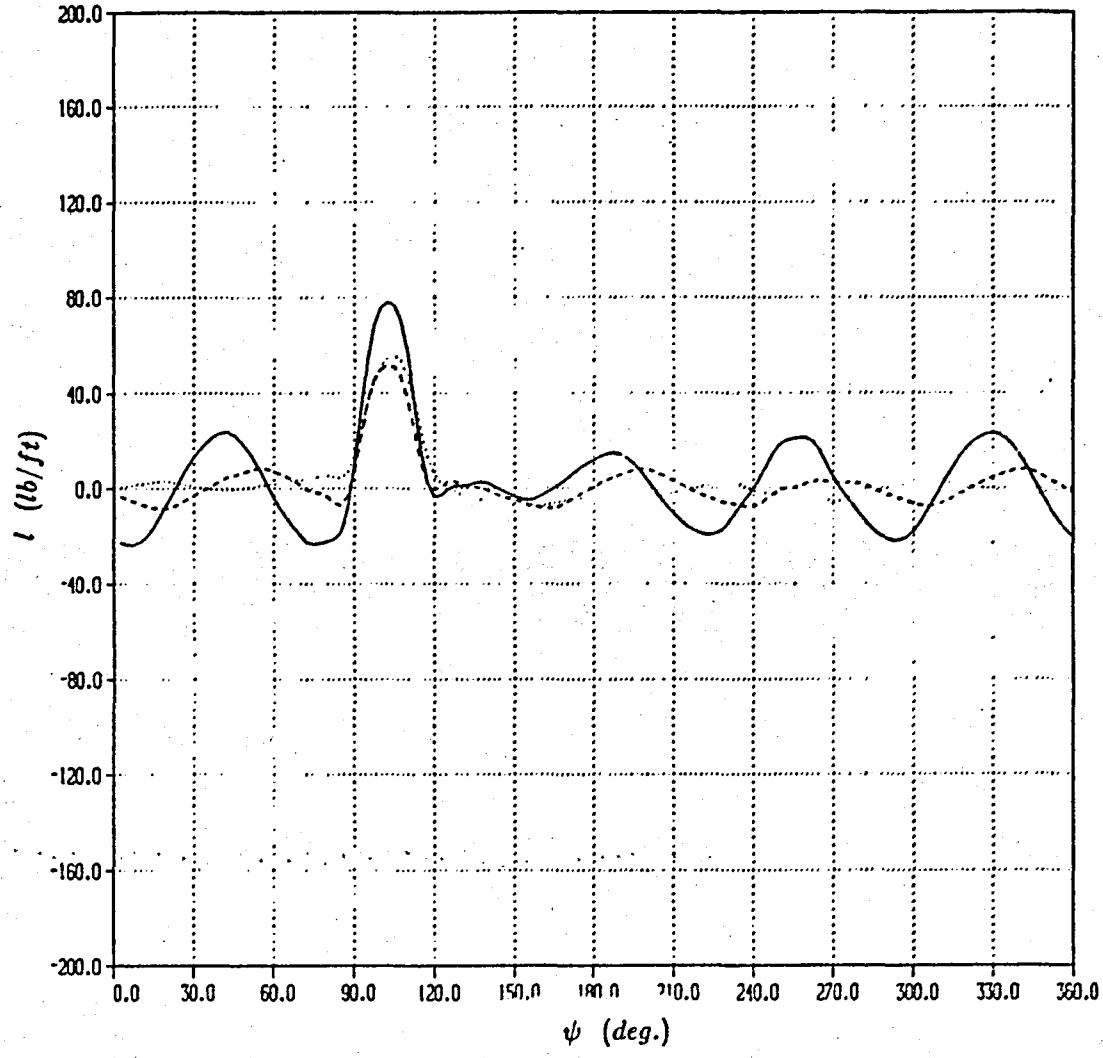

Figure 12. Response to an air jet, HOVER

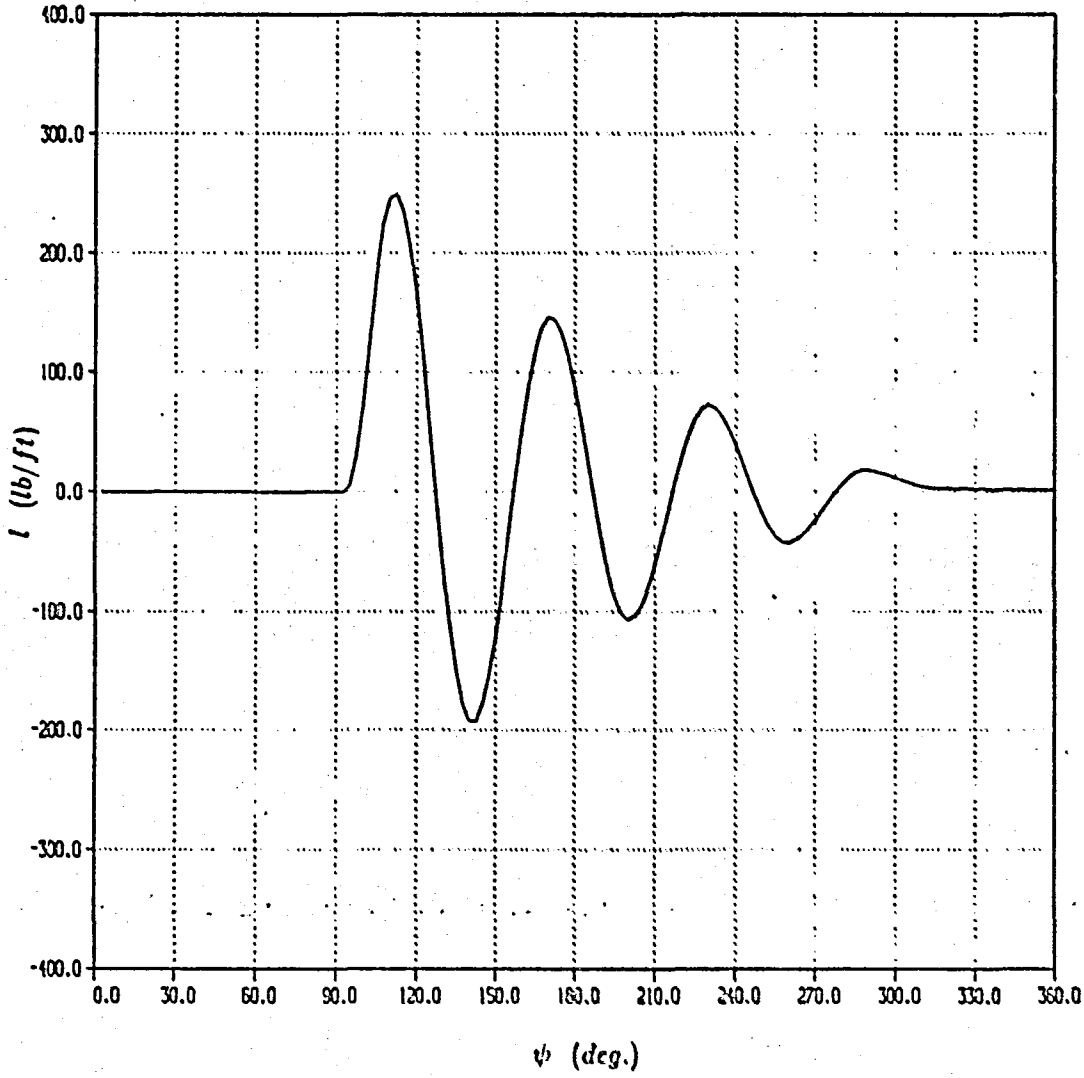

—— $b_\theta = 0.0$

Figure 13. Response to an air jet, UNSTHOVR

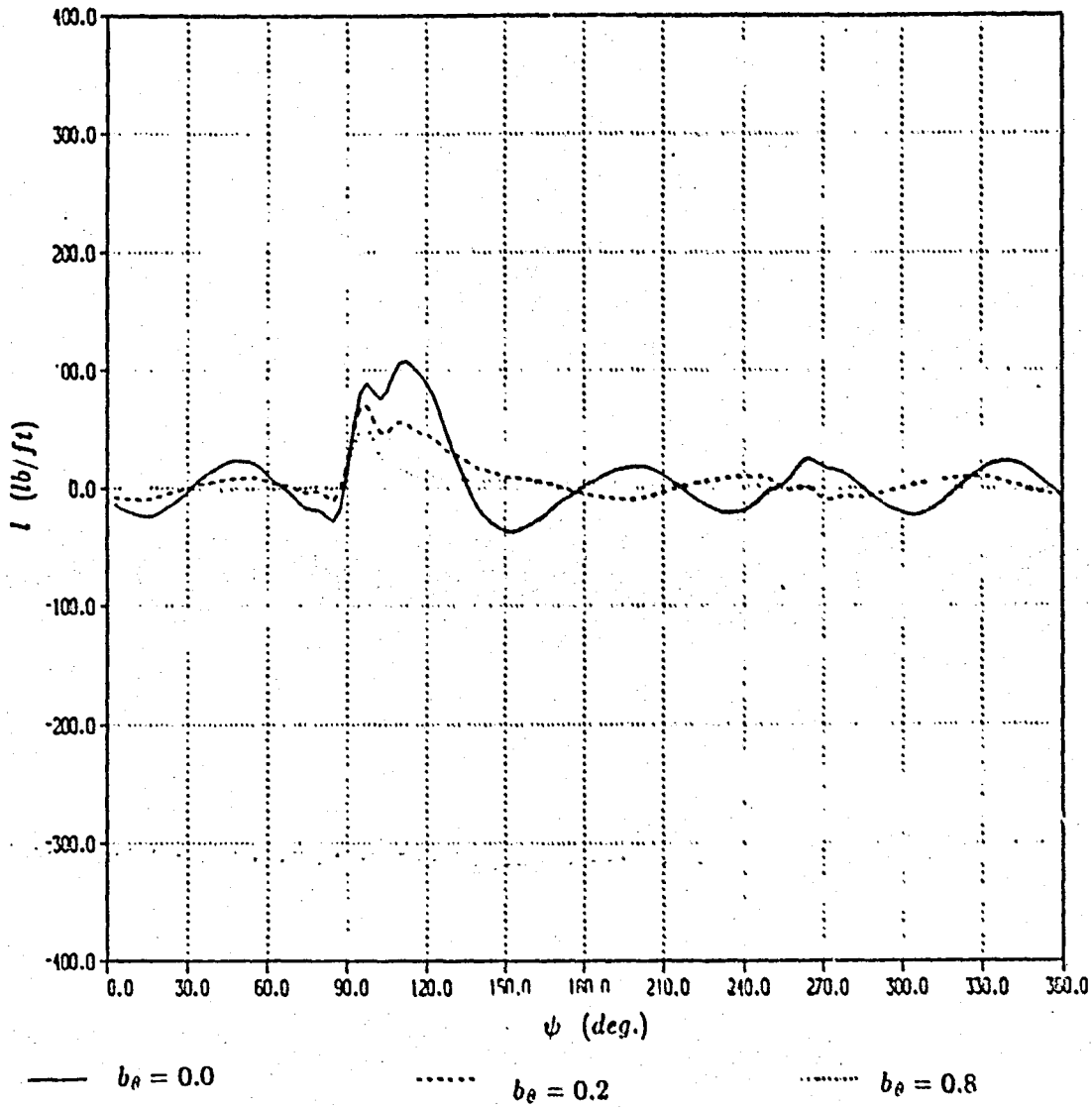

Figure 14. Natural frequency of the system

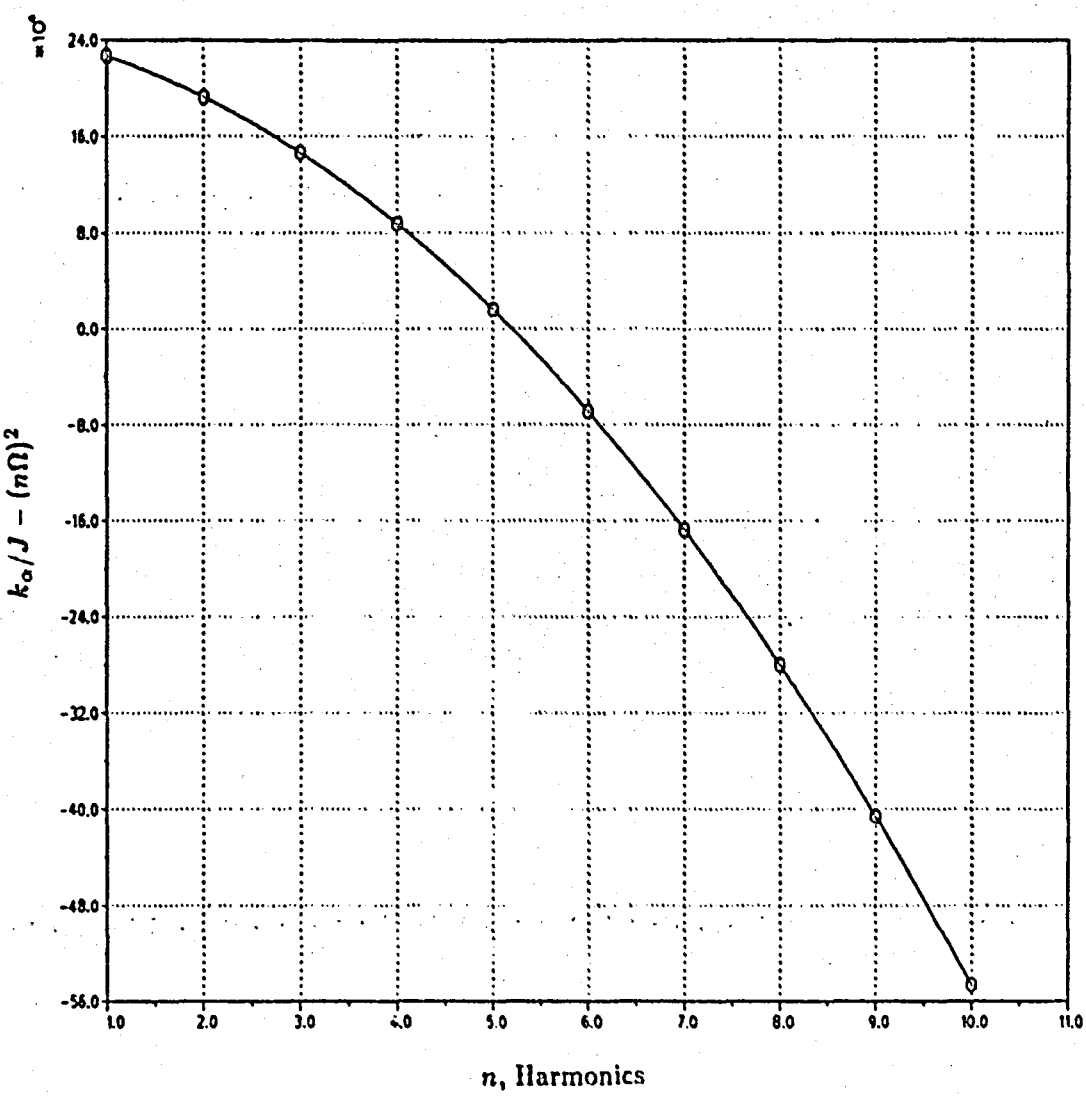

Figure 15. Effect of friction, fixed tip inflow set

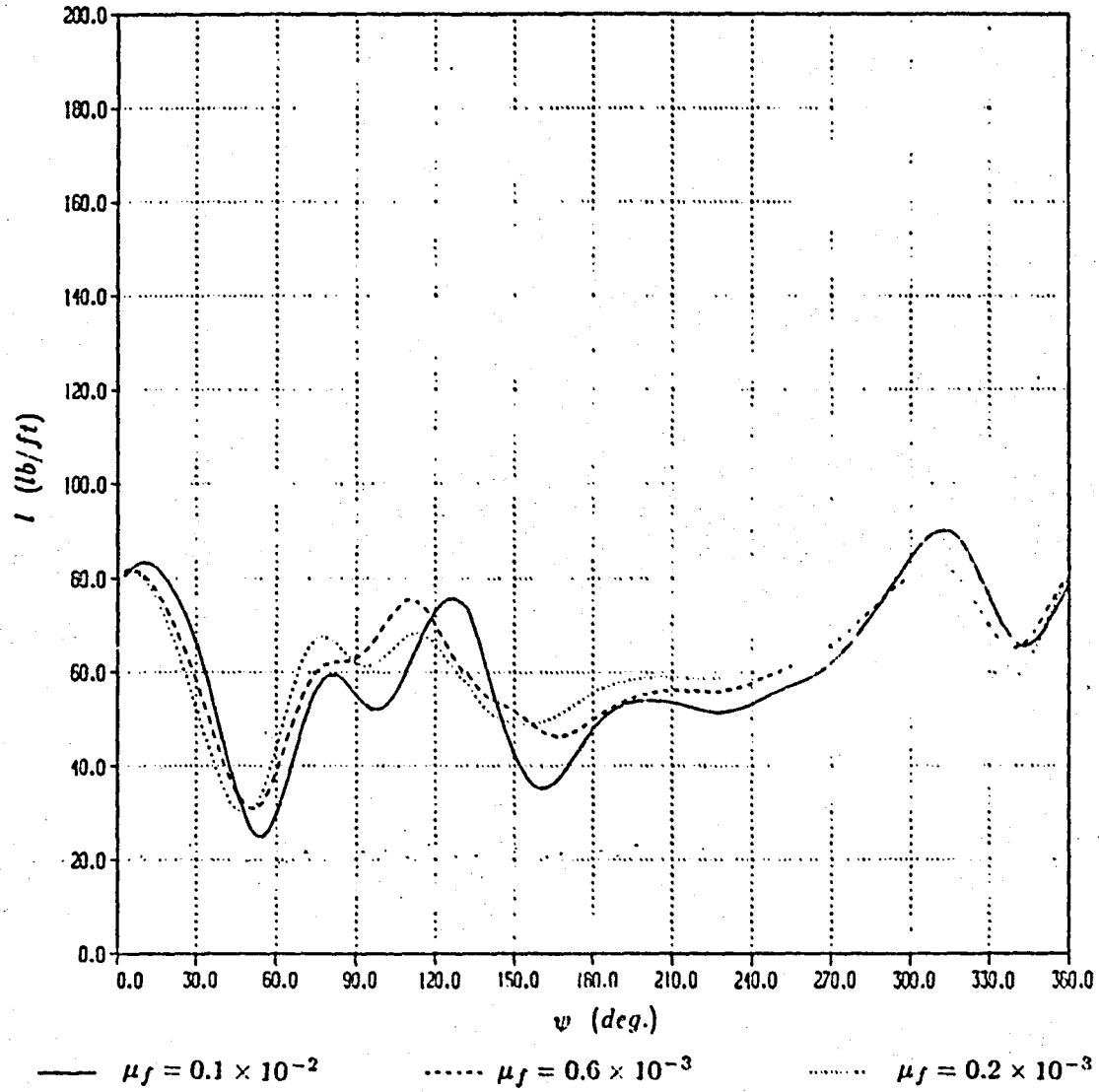

Figure 16. Effect of mechanical damping, fixed tip inflow set

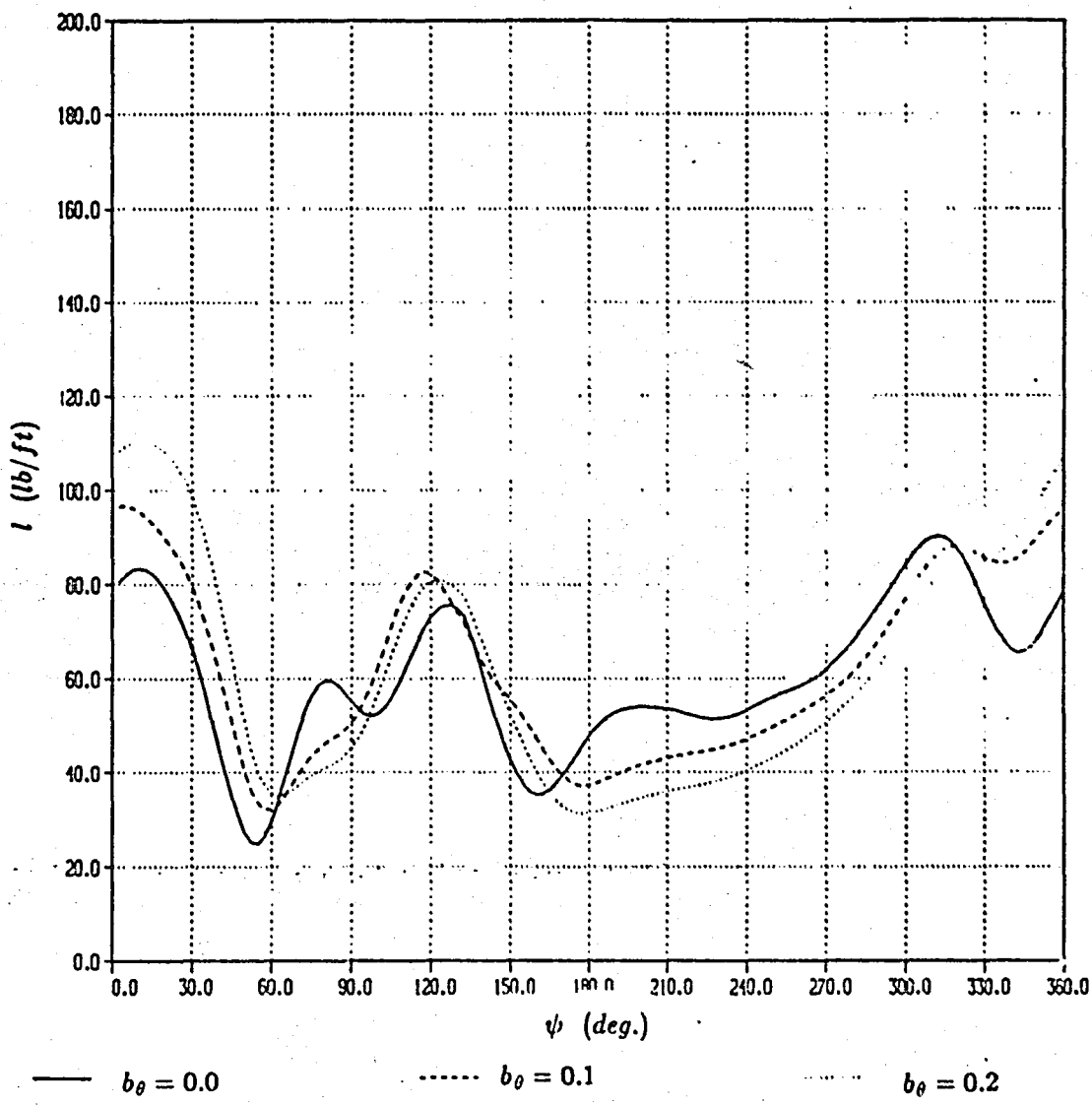

Figure 17. Effect of a mechanical spring, fixed tip inflow set

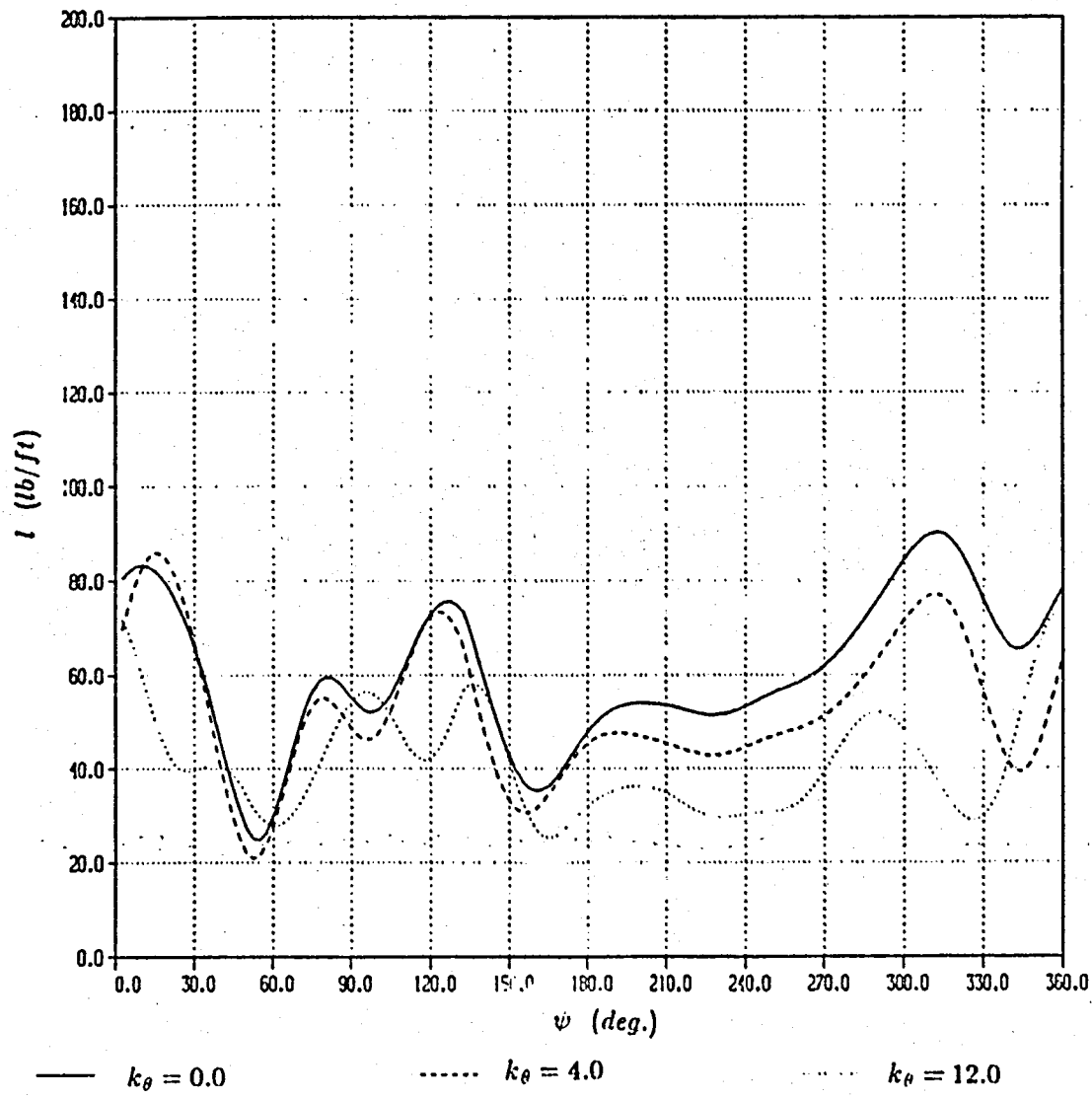

Figure 18. Effect of friction, free-tip inflow set

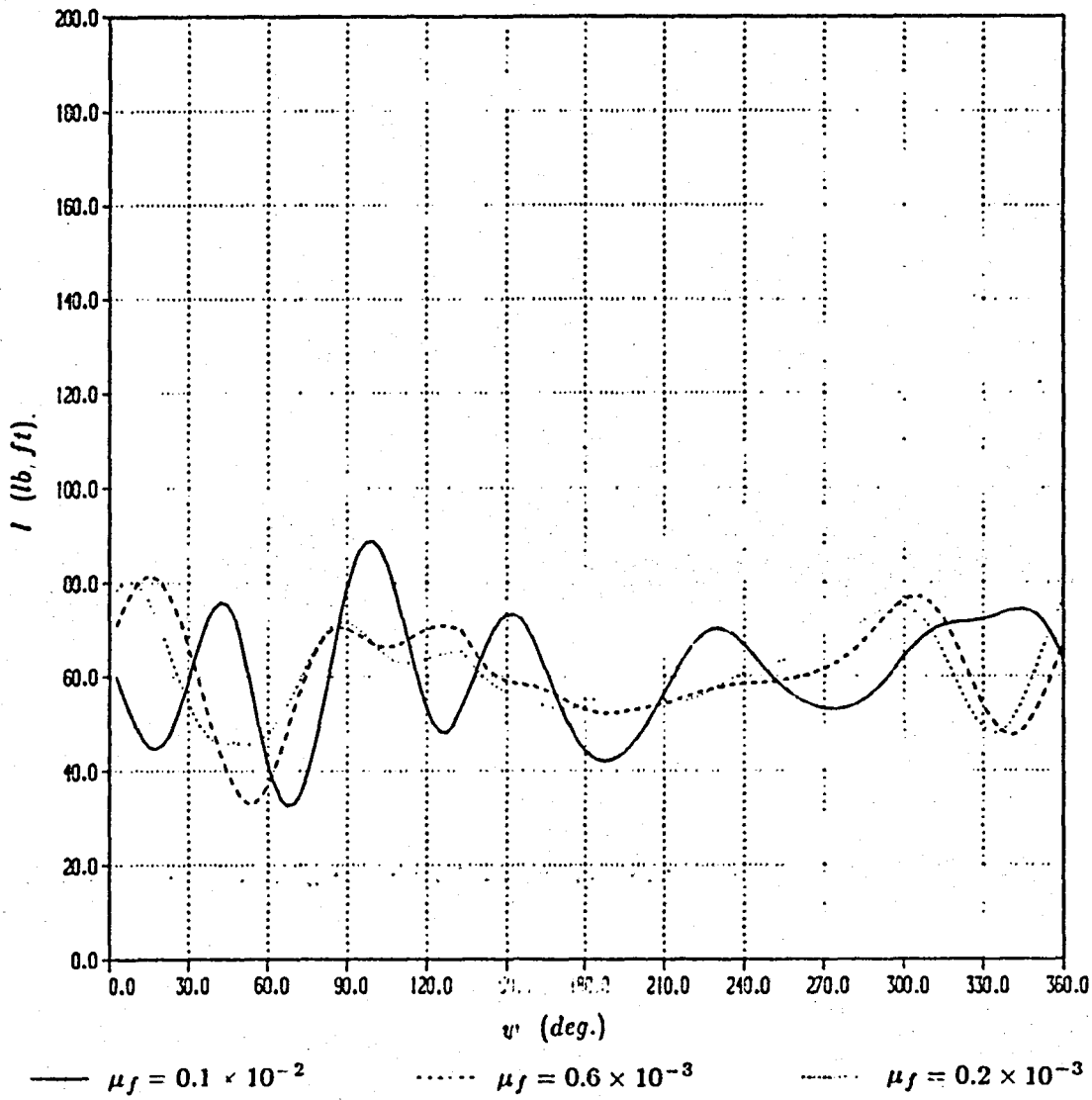

Figure 19. Effect of mechanical damping, free-tip inflow set

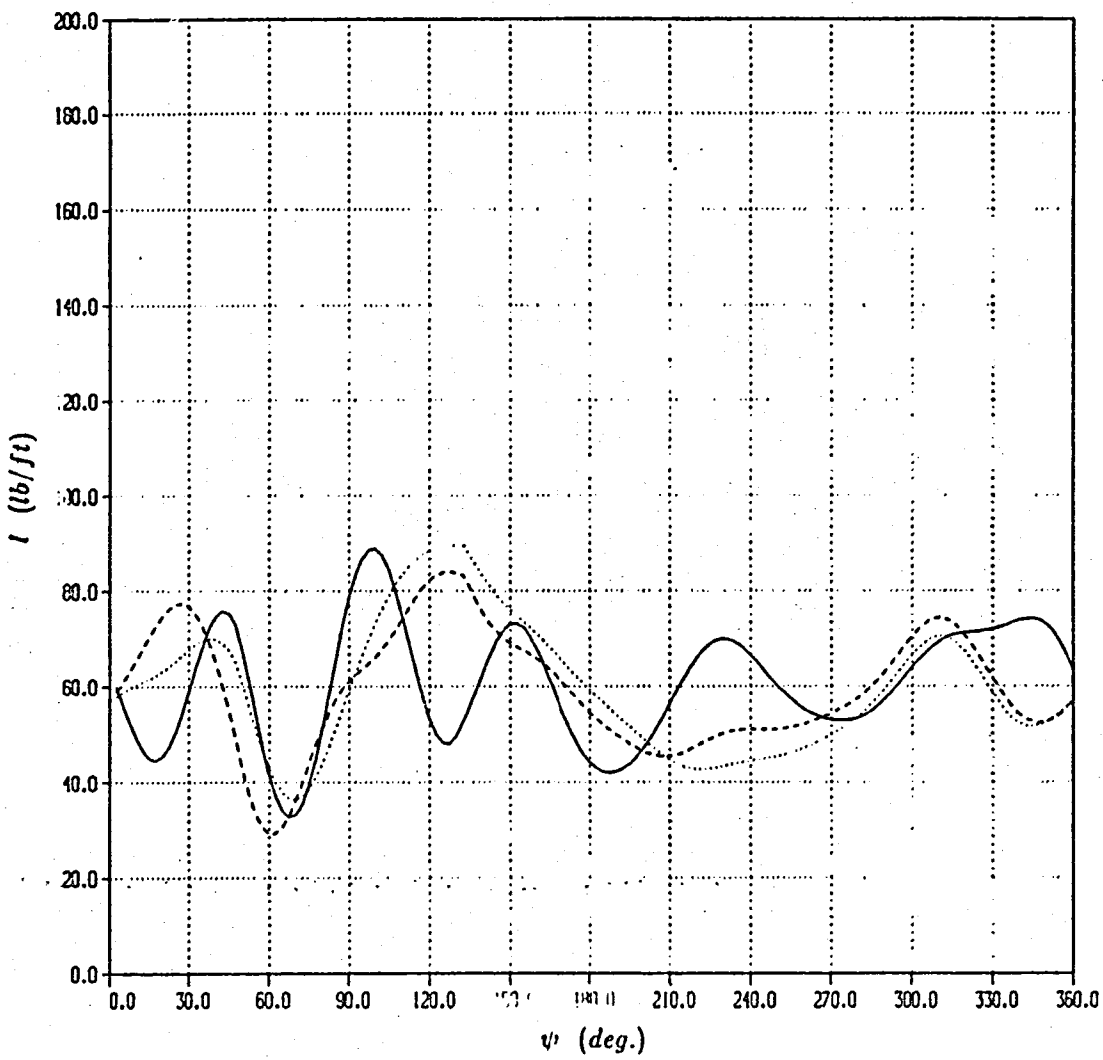

Figure 20. Effect of a mechanical spring, free-tip inflow set

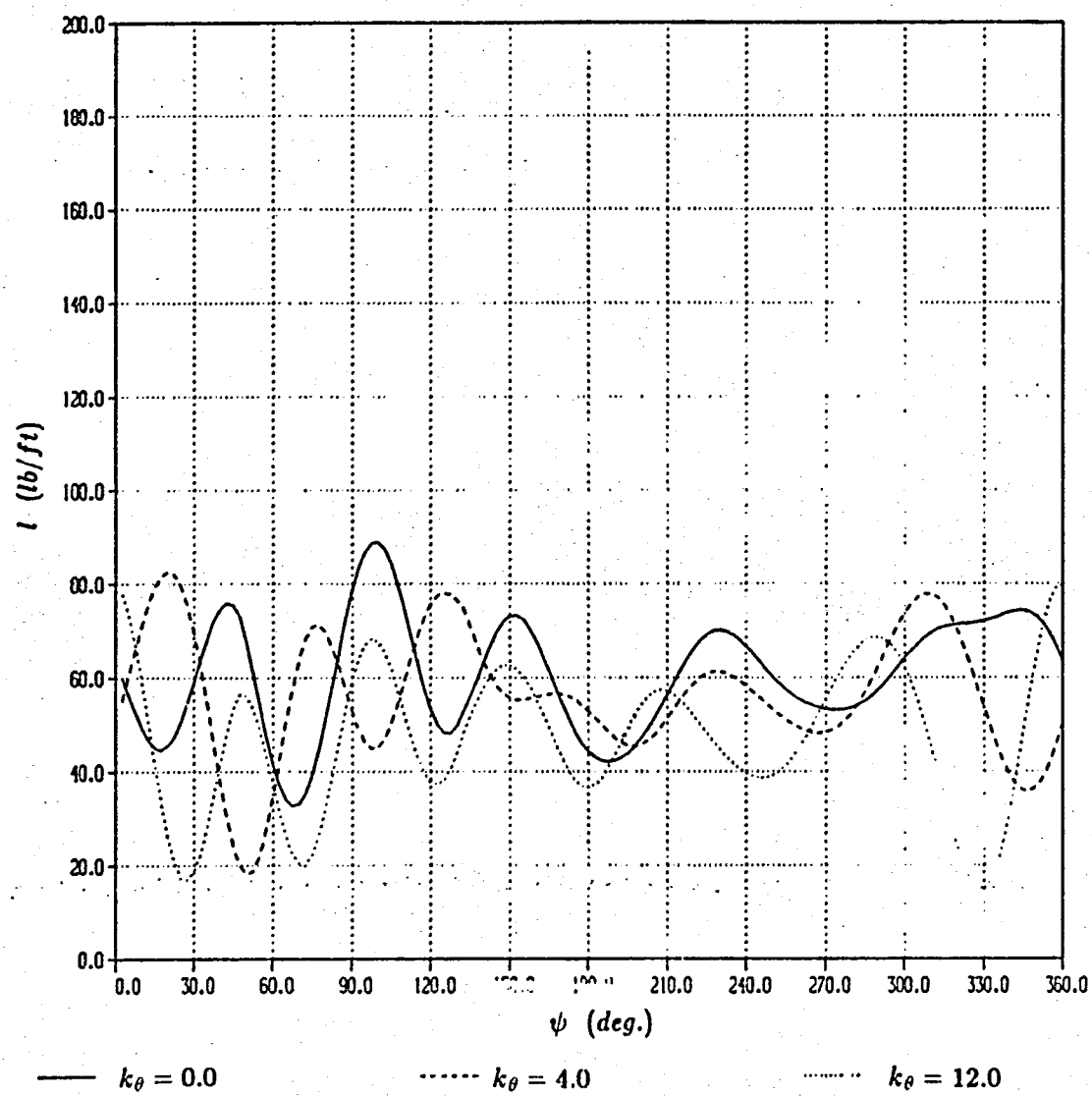

Figure 21. Pitch angle of the free-tip with fixed tip inflow set

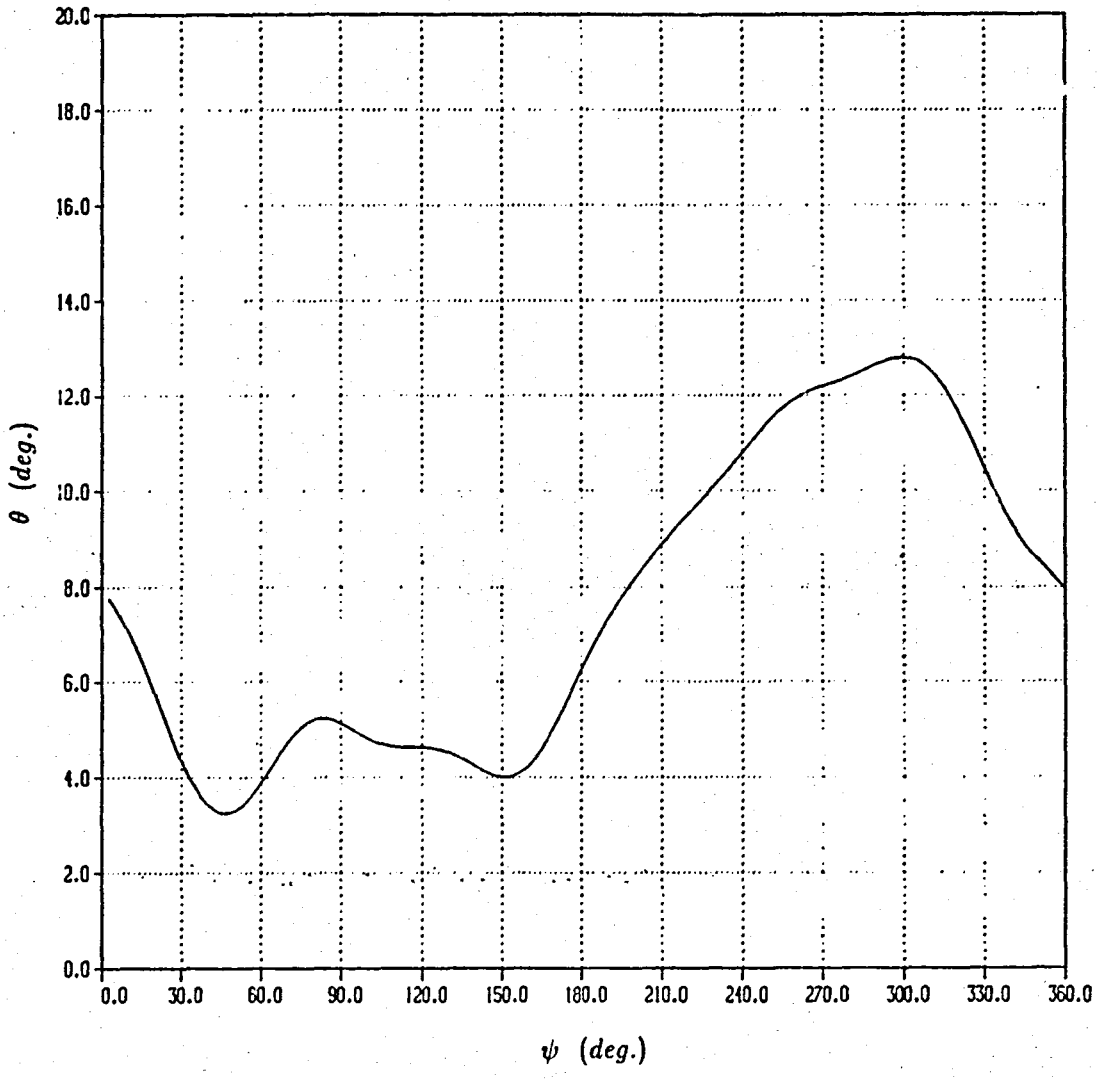

Figure 22. Pitch angle of the free-tip with free-tip inflow set

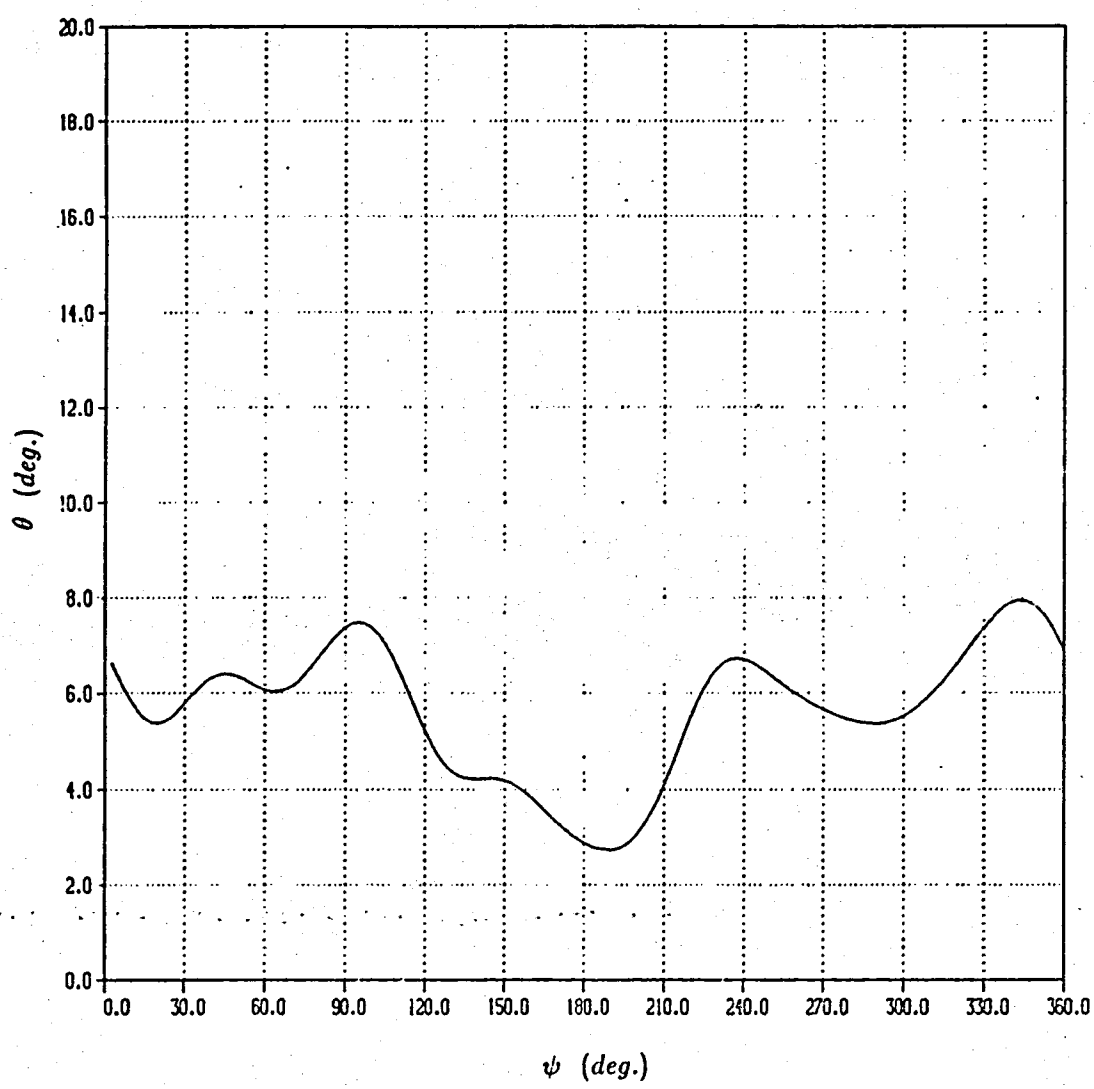

Figure 23. Effect of friction

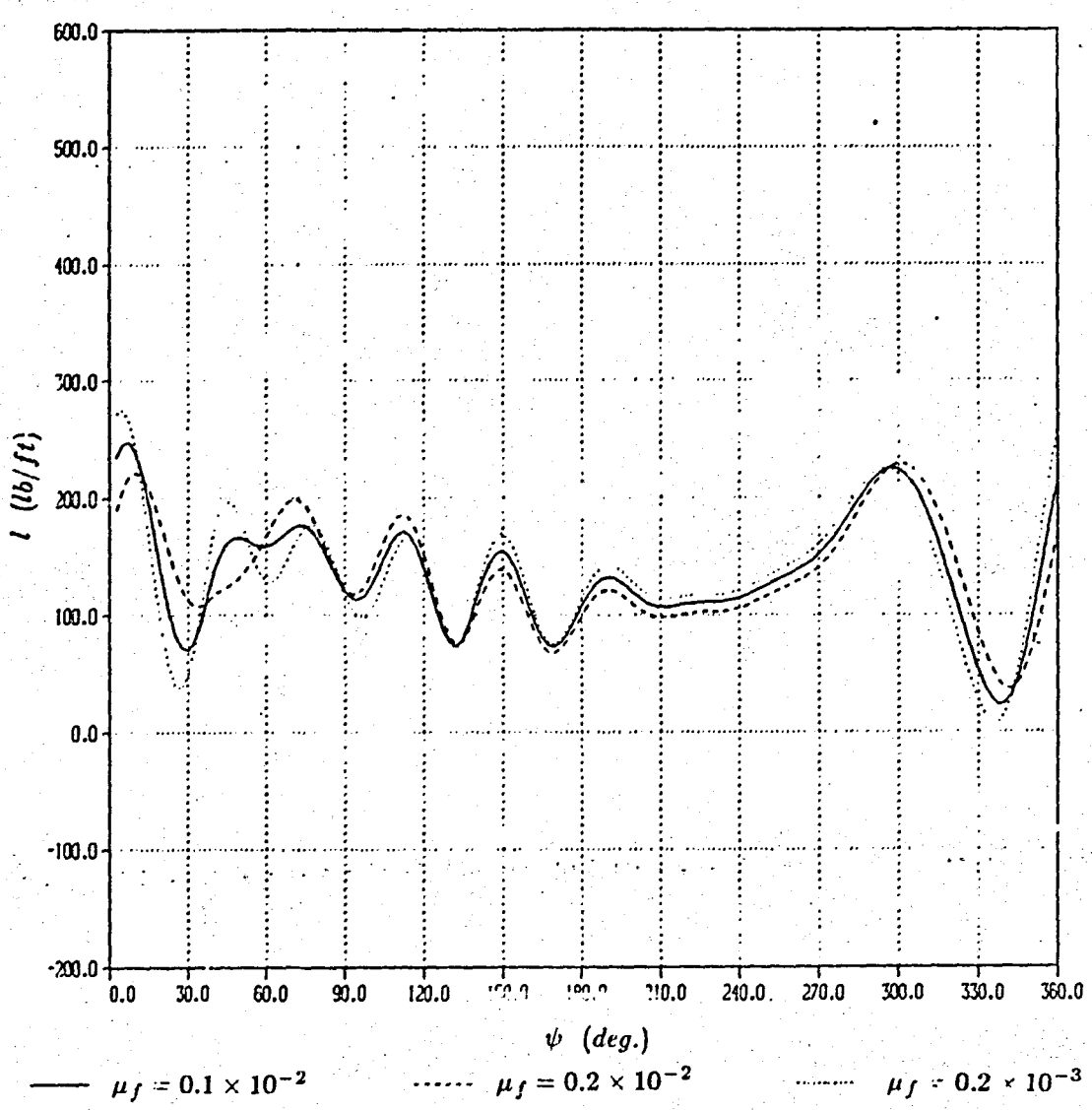

Figure 24. Effect of mechanical damping

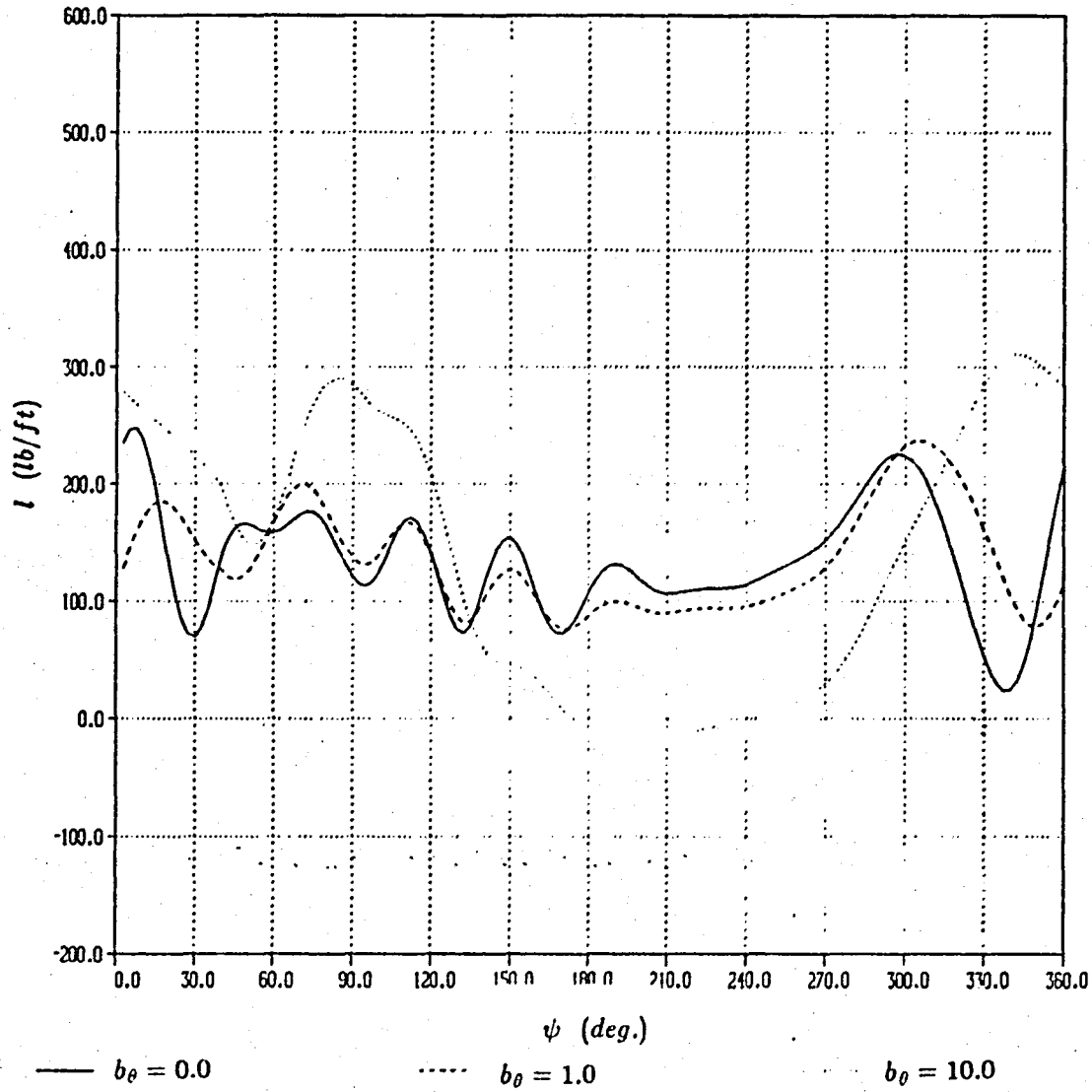

Figure 25. Effect of a mechanical spring

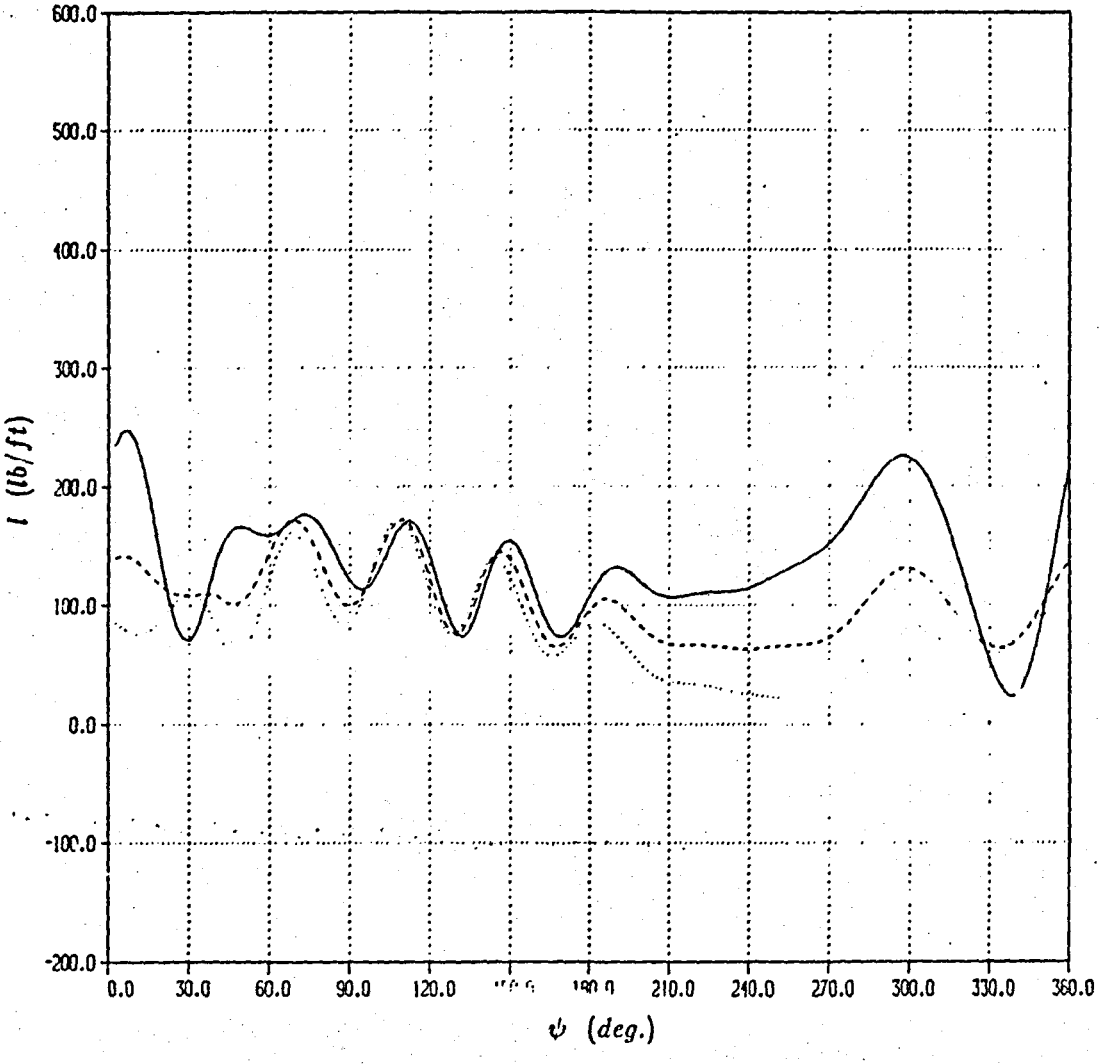

Figure 26. Effect of the effective pitch axis

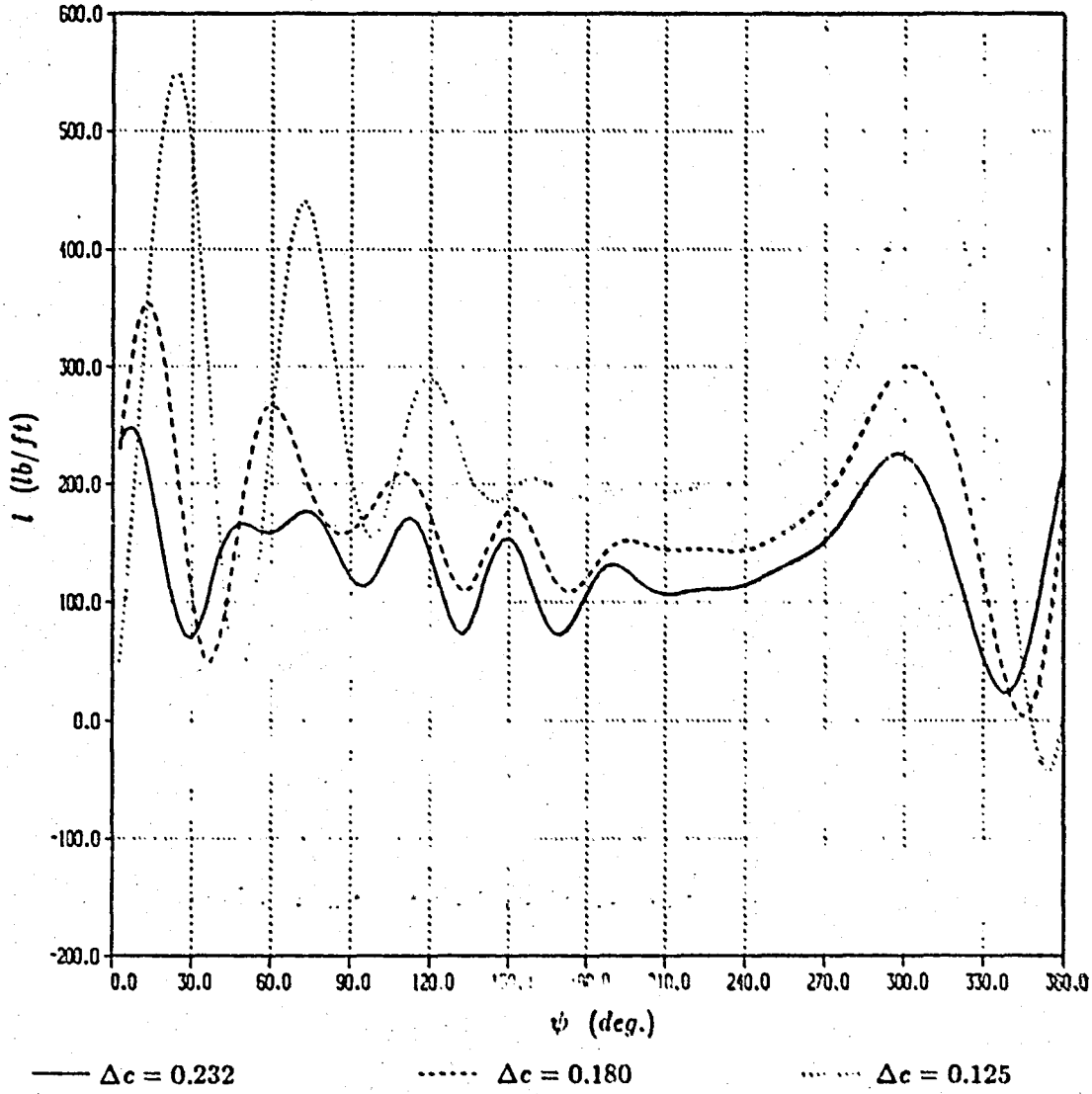

Figure 27. Effect of the constant control moment

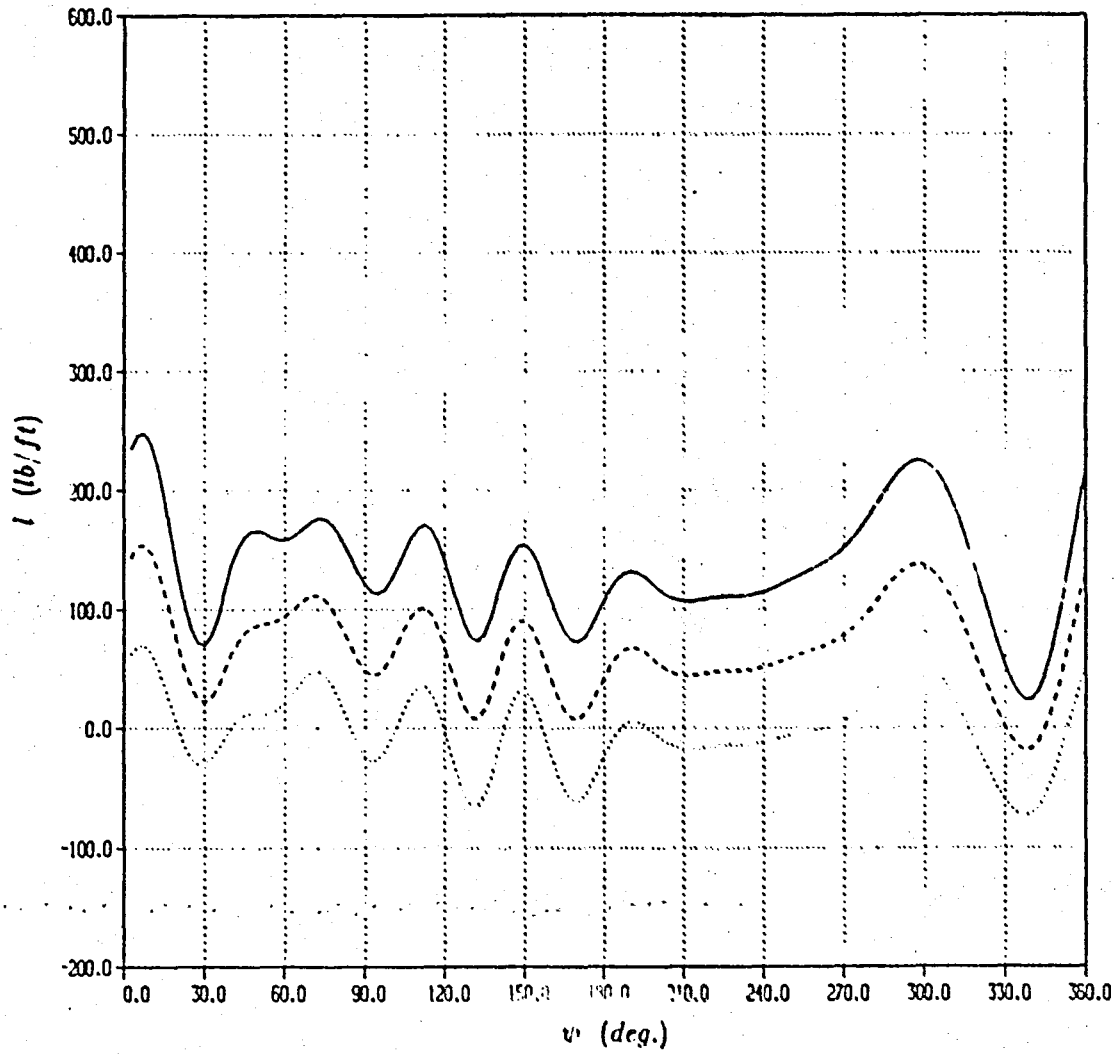

Figure 28. Effect of the aerodynamic moment coefficient

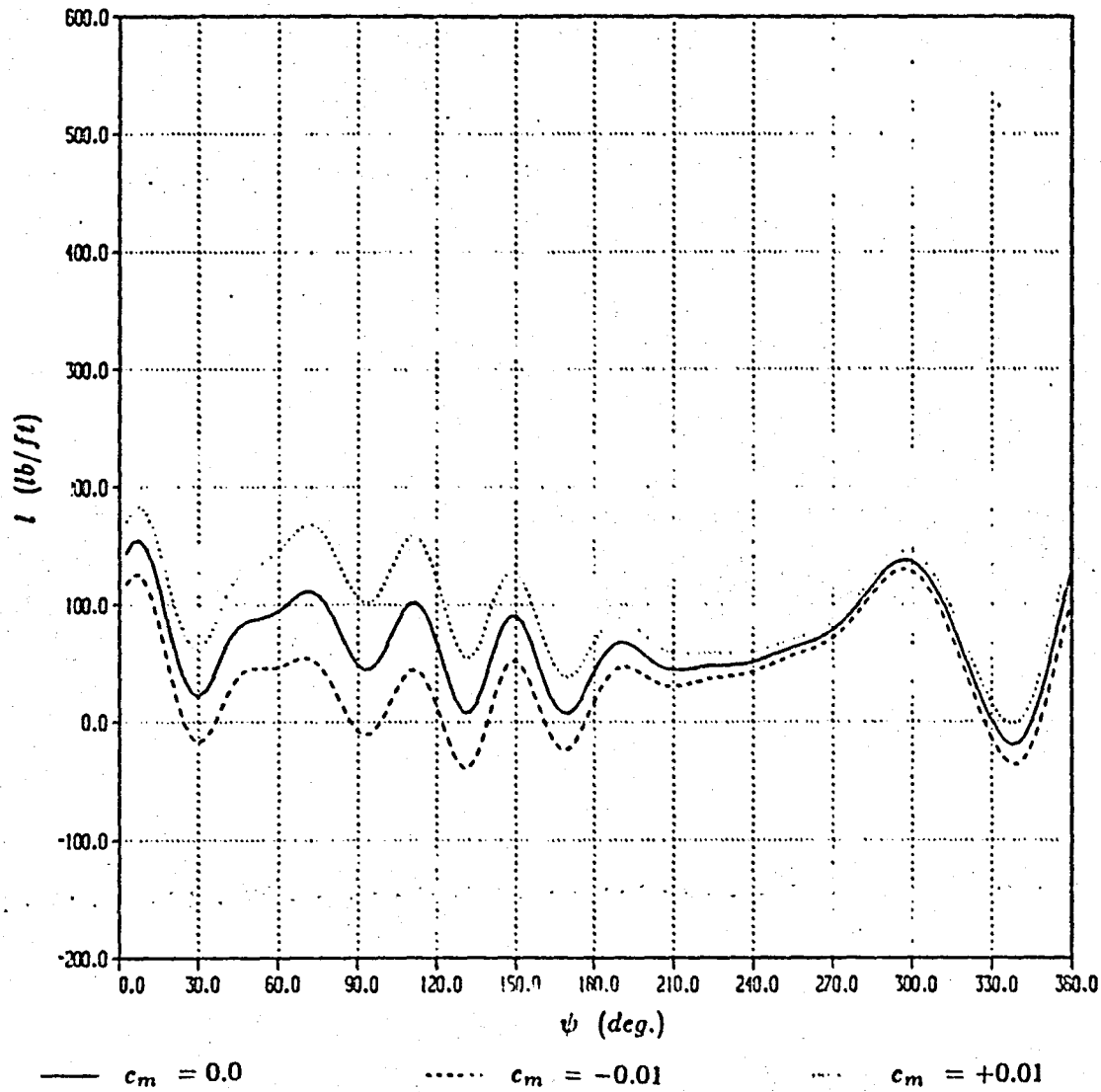

Figure 29. Effect of mechanical damping and mechanical spring

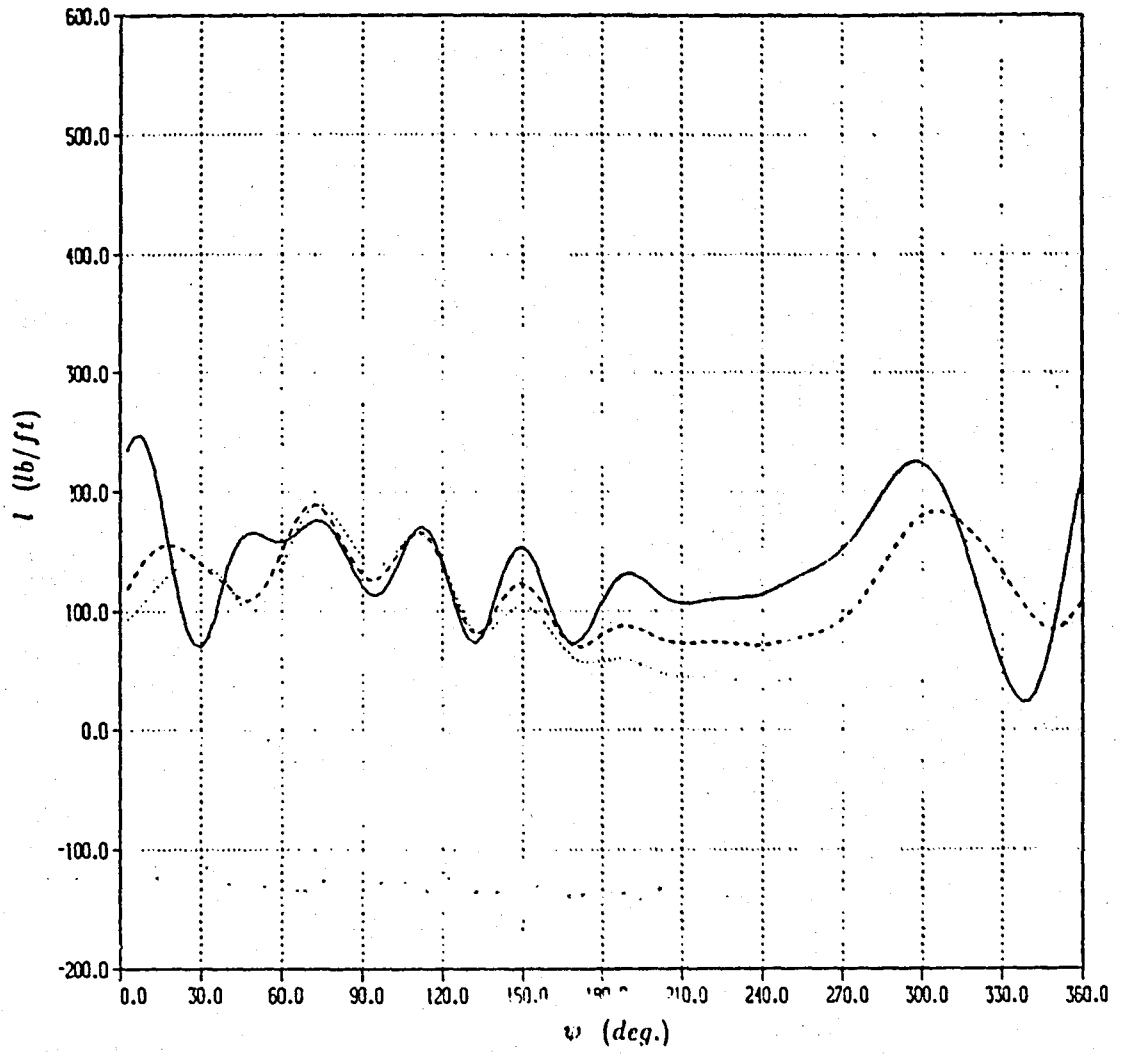

Figure 30. Effect of mechanical damping, $\mu = 0.15$

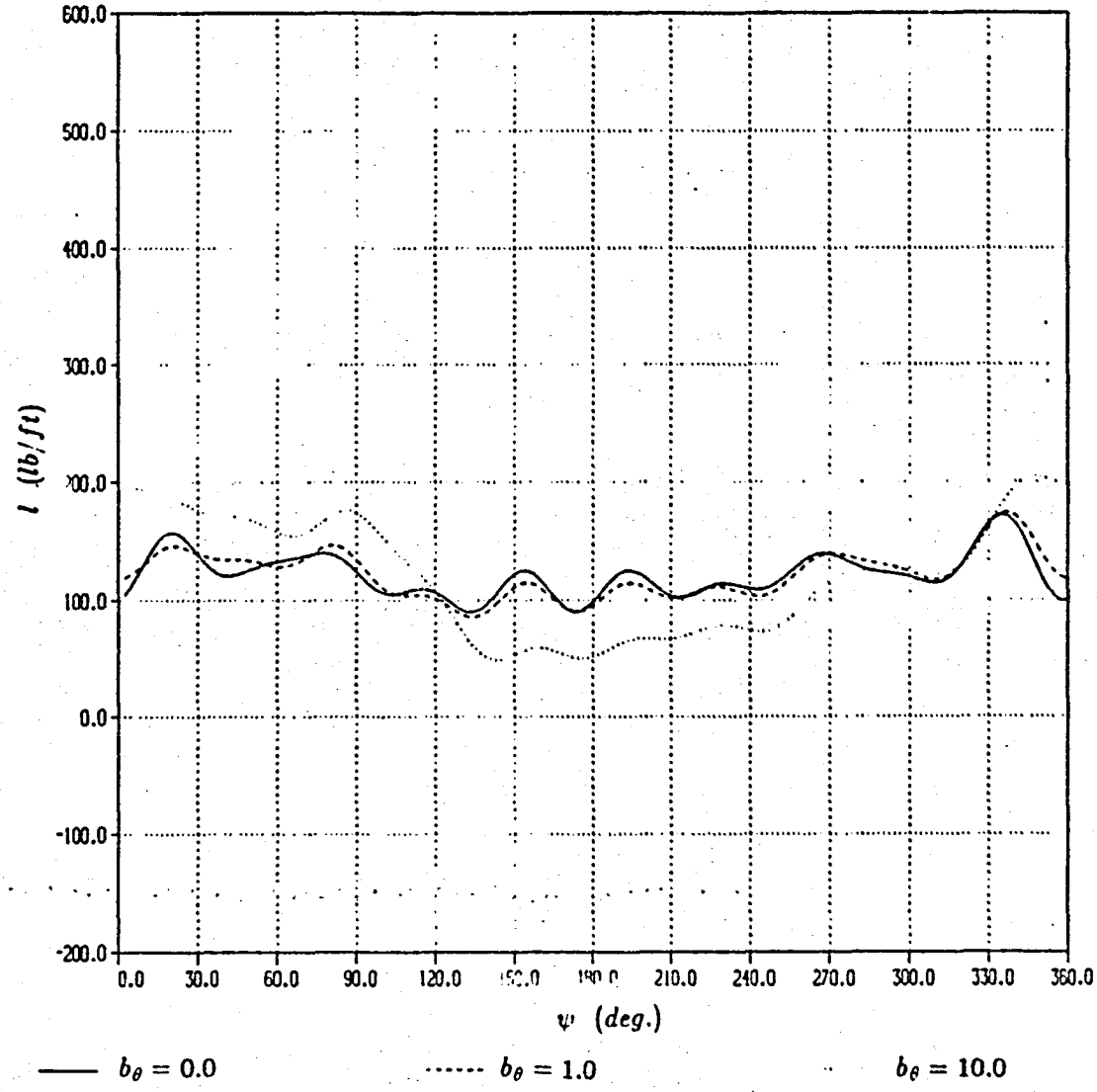

Appendix A. Input Data for UNSTEADY

Sample Data Set

```
$SUSIE  NMAX=20, EPS=0.00001
N=144,J=.02,DELC=0.232,CPA=0.125,C=1.2657,
QMSQ=1436.36, VSOUND=1143.75, V=192.3, OR=650.0, RADIUS=28.0,
MASS=0.18634, QZERO=40.0, A1=0.0, B1=0.0, CMO=0.0,PHIZ=7.43125,
BETA0=0.0,D1=-5.63269,D2=3.75692,D3=0.94621,D4=-0.52683,D5=-0.46910,
D6=0.09259, D7=0.18116, D8= 0.14434, D9=-0.05879, D10=-0.16852,
F1=0.62908, F2=-0.53383, F3= 0.32642, F4= 0.36417, F5=0.14365,
F6=-0.11166, F7= 0.09747, F8=0.20000,F9=-0.00475, F10=-0.00700,
BS1=.0, BS2=0.0, BS3=0.0, BS4=0.0, BS5=0.0,
BS6=0.0, BS7=0.0, BS8=0.0, BS9=0.0, BS10=0.0,
BC1=0.0, BC2=0.0, BC3=0.0, BC4=-0.0, BC5= 0.0,
BC6=0.0, BC7=0.0, BC8=0.0, BC9=0.0, BC10=0.0,
CLA0=3.552, DIVMAC=0.75,
CD0=0.0084, CD1=-0.0102, CD2=0.384, MACRIT=0.83, ACRIT=33.,
DCDDM=.05, MUL=0.001, BDOTH=0.0, KTHETA=0.0,
MA=0.004415, MF=0.016490, LA=0.28, LF=0.075,
AP0= 22.71, AP1=-2.23, BP1=13.28, TW=-8.0, TLOC=25.20,
TIPL=2.8,   GAMMA=0.0, THPRE=0.0 $END
```

Input Data Description

NMAX	maximum number of iterations
EPS	limit on $\alpha_{n+1} - \alpha_n$ (rad)
N	number of computation points
J	moment of inertia of Free-Tip $(slug\ ft/ft)$
DELC	effective pitch axis offset, Δc
CPA	location of the pitch axis measured from the leading edge
C	Free-Tip average chord length (ft)
QMSQ	dynamic pressure/(Mach number)^2 (lb/ft^2)
VSOUND	sonic velocity (ft/sec)
V	helicopter forward flight velocity (kts)
OR	average tip speed (ft/sec)

RADIUS	rotor radius (ft)
MASS	mass of the Free-Tip $(slug/ft)$
QZERO	constant control moment $(ft\ lb/ft)$
A1, B1	cyclic control moment $(ft\ lb/ft)$
CMO	constant moment coefficient
PHIZ, D1-D10 F1-F10	harmonic coefficients which define the inflow angle distribution (deg)
BSN1-BSN10, BCS1-BCS10	harmonic coefficients which define the flapping motion (deg)
CLAO	lift curve slope of the tip section at $M_\infty = 0$
DIVMAC	lift divergence Mach number (See listing.)
CDO,CD1,CD2	coefficients which define the drag coefficient as a function of α
VMCRIT,ACRIT	critical α and Mach number used to define the compressibility drag increment
DCDDM	$\frac{\partial C_d}{\partial M}$ at critical Mach number, VMCRIT
MUL	friction coefficient
BDOTH	mechanical damping factor $(lb\ sec^2/ft)$
KTHETA	mechanical spring rate $(lb\ ft/ft)$
MA, MF	forward and aft masses which contribute to the feathering moment $(slug/ft)$
LA, LF	forward and aft moment arms which contribute to the feathering moment (ft)
APO, AP1, AP2	collective and cyclic pitch control of the inboard section, measured at the blade root in the shaft axis system (deg)
TW	blade twist, negative down (deg)

TLOC	radial location of the Free-Tip c. g. *(ft)*
TIPL	Free-Tip span length *(ft)*
GAMMA	Free-Tip dihedral angle, positive down *(deg)*
THPRE	mechanical spring pretwist angle *(deg)*

Appendix B. Input Data for UNSTHOVR

Sample Data Set

```
$SUSIE  NMAX=40, EPS=0.00001
N=144,J=.000388,DELC=.13,CPA=.125,C=.56077
QMSQ=1439.37, VSOUND=1137.73, V=0.0, OR=700.0, RADIUS=8.4,
MASS=0.01157, QZERO=0.0, A1=0.0, B1=0.0, CM0=0.,
CLA0=3.552, DIVMAC=0.75,
CD0=0.0101, CD1=-0.008, CD2=0.075, VMCRIT=0.706, ACRIT=32.2,
DCDDM=0.105, MUL=0.001, BDOTH=0.0, KTHETA=0.0,
MA=0.0001012, MF=0.001133, LA=0.084, LF=0.0075,
AP0= -6.48, AP1=0.0, BP1=0.0, TW=-9.450, TLOC= 7.56,
TIPL=0.84,   GAMMA=0.0, THPRE=0.0, PHIA=3.0,PHIB=0.0,PSTART=90.,
PEND=120.0 $END
```

Input Data Description

NMAX	maximum number of iterations
EPS	limit on $\alpha_{n-1} \quad \alpha_n$ (rad)
N	number of computation points
J	moment of inertia of Free-Tip $(slug\ ft, ft)$
DELC	effective pitch axis offset, Δc
CPA	location of the pitch axis measured from the leading edge
C	Free-Tip average chord length (ft)
QMSQ	dynamic pressure/(Mach number)^2 (lb/ft^2)
VSOUND	sonic velocity (ft/sec)
V	helicopter forward flight velocity (kts), must be 0
OR	tip speed (ft/sec)

RADIUS	rotor radius (ft)
MASS	mass of the Free-Tip $(slug/ft)$
QZERO	constant control moment $(ft\ lb/ft)$
A1,B1	cyclic control moment $(ft\ lb/ft)$
CMO	constant moment coefficient
CLAO	lift curve slope of the tip section at $M_\infty = 0$
DIVMAC	lift divergence Mach number
CDO,CD1,CD2	coefficients which define the drag coefficient as a function of α
VMCRIT,ACRIT	critical α and Mach number used to define the compressibility drag increment
DCDDM	$\frac{\partial C_d}{\partial M}$ at critical Mach number, VMCRIT
MUL	friction coefficient
BDOTH	mechanical damping factor $(lb\ sec^2/ft)$
KTHETA	mechanical spring rate $(lb\ ft/ft)$
MA,MF	forward and aft masses which contribute to the feathering moment $(slug/ft)$
LA, LF	forward and aft moment arms which contribute to the feathering moment (ft)
APO,AP1,AP2	collective and cyclic pitch control of the inboard section, measured at the blade root in the shaft axis system (deg)
TW	blade twist, negative down (deg)
TLOC	radial location of the Free-Tip c. g. (ft)
TIPL	Free-Tip span length (ft)

GAMMA	Free-Tip dihedral angle, positive down (*deg*)
THPRE	mechanical spring pretwist angle (*deg*)
PHIA	amplitude of half sine inflow angle (*deg*)
PHIB	constant inflow angle (*deg*)
PSTART	azimuthal angle at which the half sine inflow angle begins (*deg*)
PEND	azimuthal angle at which the half sine inflow angle ends (*deg*)

End of Document